1996

A Multiphase Mathematical Model of a Nickel/Hydrogen Cell

Pauline De Vidts
Texas A & M University - College Station

Publication Info

Published in *Journal of the Electrochemical Society*, Volume 143, Issue 10, 1996, pages 3223-3228.

De Vidts, P., Delgado, J., & White, R.E. (1996). A Multiphase Mathematical Model of a Nickel/Hydrogen Cell. *Journal of the Electrochemical Society*, *143*(10) 3223-3228.
Publisher's Version: http://dx.doi.org/10.1149/1.1837190

A Multiphase Mathematical Model of a Nickel/Hydrogen Cell

Pauline De Vidts,* Javier Delgado, and Ralph E. White*

Department of Chemical Engineering, University of South Carolina, Columbia, South Carolina 28209, USA

ABSTRACT

A mathematical model for a nickel/hydrogen cell is developed to investigate the dynamic performance of the cell's charge and discharge processes. Concentrated solution theory and the volume averaging technique are used to characterize the transport phenomena of the electrolyte and other species in the porous electrode and separator. Other physical fundamentals, such as Ohm's law, are employed to describe the electrical and other physical processes in the cell. The model is designed to predict the distribution of electrolyte, hydrogen, and oxygen concentrations within the cell, hydrogen and oxygen pressure, potential, current density, electrochemical reaction rates, and state of charge. The model can be used to evaluate the influences of all the physical, design, and operation parameters on the behavior of a nickel-hydrogen cell. The model simulations show excellent agreement with experimental data for charge and discharge operations. The model simulations show the formation of a secondary discharge plateau by the end of discharge. This plateau is caused by oxygen reduction at the nickel electrode. It is the first model that predicts this feature, which is a characteristic of the nickel electrode. The model simulations also show the existence of an optimum charge rate that maximizes the charge efficiency, which can be used for the implementation of optimal operating conditions.

Introduction

In this article we present a mathematical model for a nickel/hydrogen cell ($NiOOH/H_2$) for charge and discharge operations. The nickel/hydrogen battery has several attractive features that make it the prime candidate for energy storage in many aerospace applications. Salient features of this battery are a long cycle lifetime that exceeds any other maintenance-free secondary battery system, high specific energy (energy/weight), high power density, and tolerance to overcharge.[1]

The nickel/hydrogen technology is relatively new and there is extensive research being done to improve its general performance and develop battery designs for specific applications. Most of these studies consist of experimental testing of battery designs under various conditions of operation. The process of designing a battery based on experimental testing is lengthy and costly, because there are many variables and parameters that can be modified. A mathematical model of the $NiOOH/H_2$ battery based on fundamental principles can be used to study the effect of various parameters and operating conditions on the battery's performance. Therefore, such a model can help researchers and battery engineers in the development of new or improved battery designs for specific applications, saving resources that otherwise would be dedicated to experimental testing.

Some researchers have modeled the nickel electrode either alone[2-4] or included in a cell.[5-8] Among the existing models for the NiOOH electrode, the most successful ones are those developed by Bouet *et al.*[4] and Mao *et al.*[8] They developed pseudo-two-dimensional models for the discharge of the electrode. Their models include the mass transfer and ohmic resistance in the electrolyte and the proton diffusion in the solid active material of the nickel electrode. Many researchers have identified the proton diffusion process as a controlling phenomenon on the nickel electrode's behavior.[9-12] The simulations from both models[4,8] agree qualitatively with experimental observations on the nickel electrode behavior. In particular, the simulations show the decrease in active material utilization as the discharge current is increased; a simulation capability not held by previous models. Recently, De Vidts and White[13] presented a model for a nickel/cadmium cell that includes proton diffusion in the NiOOH electrode. The simulations from this model showed the same positive results as those from the models by Bouet *et al.*[4] and Mao *et al.*[8] A sensitivity analysis of the model parameters[13] showed that during discharge the cell potential is affected mostly by the kinetics of the main reaction in the nickel electrode. As the discharge proceeds, the proton diffusion becomes important along with the kinetics of the main reaction. The results also showed that the proton diffusion is the most important factor that affects the utilization of the active material.

Despite the efforts of previous researchers, there is one feature that the models mentioned above have not been able to predict. Cells that have a nickel electrode of the kind used in the nickel/hydrogen cell may show a second discharge plateau by the end of discharge, depending on the operating conditions. Some researchers think that this second plateau may be caused by the formation of an insulating film at the interface between the active material and the nickel substrate,[11,14] but no definite explanation has been given in the literature.

Modeling a $NiOOH/H_2$ cell requires the representation of the processes inside the cell that have a controlling effect over its behavior. The electrodes and the separator in the $NiOOH/H_2$ cell are porous materials flooded with a concentrated binary electrolyte (KOH in aqueous solution). Therefore, the model equations are derived based on the theory for concentrated binary electrolytes[15] and the local volume averaging technique for porous media.[16] The model equations include mass transfer in three phases: liquid, gas, and solid, the kinetics of the electrochemical reactions, and equations describing the electrical behavior of the cell.

Also, the model includes the proton diffusion process in the active material of the nickel electrode. Based on experimental evidence, this process has long being thought to be an important factor affecting cells that use a nickel electrode[9-12] Two previous models, one for a nickel/cadmium cell[13] and another for the discharge of a nickel/hydrogen cell[8] show that proton diffusion may be the main factor affecting the utilization of active material in the nickel electrode, that is, the discharge efficiency of the cell.

The model developed here includes a gas phase inside the pores of the cell components: this phase exists in real cells but was not incorporated into previous models. Hydrogen and oxygen are produced and consumed during charge and discharge of the cell. These gases are involved in reactions on both electrodes. Thus, it is important to include in the model their transfer from one electrode to the other to evaluate the limiting role that this may have on the behavior of the cell. Predictions of the cell potential during discharge using the model show the characteristic second plateau of the nickel/hydrogen cell. This second discharge plateau is characteristic of the nickel electrode. No previous models for this type of cells produce simulations showing the second discharge plateau. The simulations show that the second plateau may be caused by oxygen reduction at the nickel electrode, which takes place by the end of discharge if there is a high concentration of oxygen.

* Electrochemical Society Active Member.

Model

Here we present the development of a mathematical model of a nickel/hydrogen cell. We begin by defining the system. We then postulate the assumptions on which the model is based and follow by presenting the model equations. The transport equations are based on the local volume averaging technique for porous media applied to porous electrodes.[17] Finally, we give the value of the parameters used for solving the model equations.

Description of the system.—A sealed nickel/hydrogen battery is a hybrid electrochemical system combining battery and fuel cell technologies. The nickel positive electrode comes from the nickel/cadmium cell, and the hydrogen negative electrode from the hydrogen/oxygen fuel cell. Sealed NiOOH/H_2 batteries are designed to contain hydrogen gas under pressure within a cylindrical pressure shell as shown in Fig. 1. Inside the pressure vessel, there are several cells connected in parallel to the outer leads (positive and negative terminals) of the battery. A cell is composed of one nickel electrode, a separator, a hydrogen electrode, and a gas screen on the back of the hydrogen electrode. The model developed in this work applies to one cell. A schematic diagram of the cell being modeled is shown in Fig. 2. The positive electrode consists of a sintered porous nickel plaque that is electrochemically impregnated with nickel hydroxide active material. The negative electrode consists of a Teflon-bonded platinum black catalyst supported on a fine mesh nickel screen with Teflon backing. The Teflon backing stops the electrolyte loss through the back side of the negative electrode while allowing hydrogen and oxygen to pass through. This keeps the reactive surface of the electrode wet with electrolyte at all times to enable the electrochemical reactions to occur. The gas screen placed behind the negative electrode consist of a mesh made of polypropylene fibers. This screen allows hydrogen and oxygen gas in the head space of the battery vessel to be transferred from and to the back of the negative electrode. The pores of the cell components are wet with an electrolytic solution consisting of a concentrated solution of KOH in water (5.8 *M*). Besides the electrolyte, the pores are filled partially with a hydrogen and oxygen gas phase.

Electrochemical reactions.—Three reactions occur simultaneously at the nickel electrode under normal operation of an NiOOH/H_2 cell. The main reaction is the oxidation/reduction of Ni species in the solid active material; side reactions are oxygen evolution/reduction and the oxidation of dissolved hydrogen. These reactions generally can be expressed as follows

$$\text{Main reaction} \quad \mathrm{NiOOH + H_2O + } e^- \underset{\text{charge}}{\overset{\text{discharge}}{\leftrightharpoons}} \mathrm{Ni(OH)_2 + OH^-} \quad [1]$$

$$\text{Side reactions} \quad \frac{1}{2}\mathrm{O_2 + H_2O} + 2e^- \rightleftarrows 2\ \mathrm{OH^-} \quad [2]$$

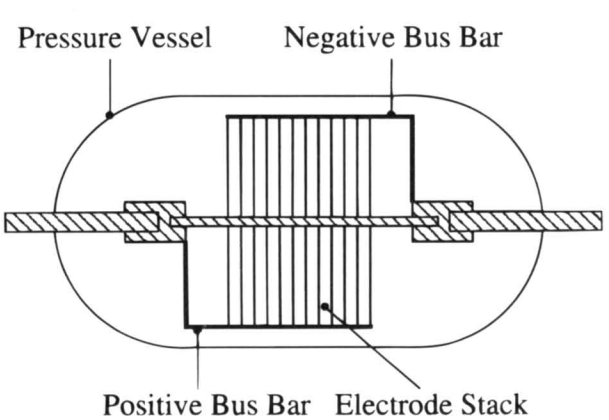

Fig. 1. Nickel/hydrogen battery.

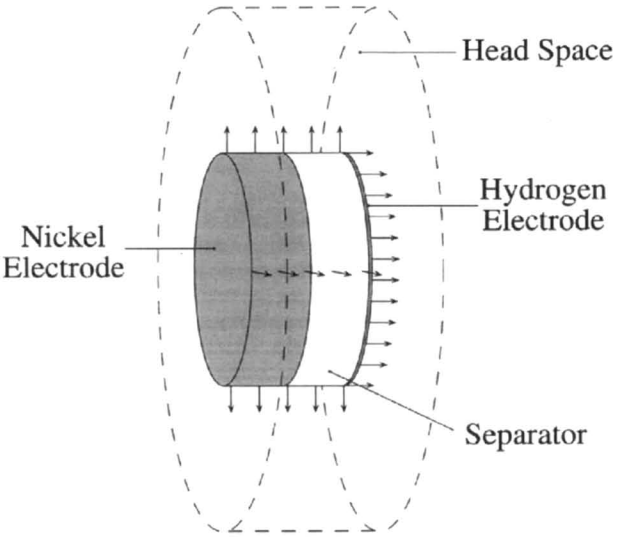

Fig. 2. Schematic diagram of the nickel/hydrogen cell modeled. Gas fluxes into the head space are shown.

$$2\mathrm{H_2O} + 2e^- \rightleftarrows \mathrm{H_2} + 2\ \mathrm{OH^-} \quad [3]$$

During charging, the applied current is used to oxidize nickel from Ni^{2+} to Ni^{3+} as shown by reaction 1. A portion of the applied current is used by oxygen evolution (reaction 2) and hydrogen oxidation (reaction 3), causing the charge efficiency to be less than 100%. On open circuit, the sum of the rates of reaction 2 and 3 must be equal to the discharge rate of NiOOH to $Ni(OH)_2$, which is equal to the self-discharge rate of the nickel electrode. During discharging, reactions 2 and 3 still occur on the nickel electrode. At the beginning of discharge the potential in the nickel electrode is high, and reaction 2 proceeds in the direction of oxygen evolution. By the end of discharge, the potential of the nickel electrode is low, and reaction 2 may proceed in the direction of oxygen reduction if there is enough dissolved oxygen.

At the hydrogen electrode, the main reaction is hydrogen oxidation/reduction. There is also a side reaction, which is an oxygen reduction. The overall reactions can be written as

$$\text{Main reaction} \quad \mathrm{H_2 + 2\ OH^-} \underset{\text{charge}}{\overset{\text{discharge}}{\rightleftharpoons}} \mathrm{2H_2O} + 2e^- \quad [4]$$

$$\text{Side reaction} \quad 2\ \mathrm{OH^-} \rightleftarrows \frac{1}{2}\mathrm{O_2 + H_2O} + 2e^- \quad [5]$$

During charging, the applied current is used to produce hydrogen through reaction 4 and consume oxygen through reaction 5, whereas hydrogen is consumed by the applied current and the current from reaction 5 during discharging.

Assumptions.—The model developed here assumes isothermal conditions; thus, the model equations are written for mass transport only. The equations that involve the electrolytic solution are based on the theory for concentrated electrolytes,[15] because the electrolyte consists of a concentrated binary electrolyte (KOH). Fan and White[6] showed that convection effects in the electrolyte are negligible compared to the migration effects; thus, we neglect convection in the liquid phase. Also, we neglect convection in the gas phase as a first approximation, which is reasonable if the gradients in internal pressure are small.

The porosity of the nickel electrode is assumed to be constant because Fan and White[6] showed that the changes in porosity during charge and discharge of the cell are negligible. In practice, a cell is precycled (charge and discharge) several times before it is ready to be used. Hydrogen and oxygen gas are generated during precycling. This gas pushes part of the electrolyte out of the cell and creates a gas

porosity inside the nickel electrode and separator. We assume that the gas porosity is constant during operation of the cell and equal to the initial gas porosity. Therefore, the gas and liquid porosities are assumed to be constants in the nickel electrode and separator. Also, we assume that the gas phase consists of hydrogen and oxygen only; thus, we neglect the presence of water vapor in the gas phase and consider it a compressible binary mixture.

The gradients of concentration and potential in the radial direction of the cell are assumed to be negligible. Thus, the model is written in one dimension defined across the cell by the coordinate x from the center of the nickel electrode to the hydrogen electrode (see Fig. 3). Also, hydrogen ions (protons) diffuse in the solid phase of the NiOOH electrode. Enhanced imaging reveals that the structure of the nickel electrode looks like branches, all connected to each other.[1] Along the central axis of each branch is the metal substrate (nickel), which has a very high electrical conductivity, as opposed to the poorly conductive active material that surrounds the substrate, when in the $Ni(OH)_2$ form. It seems suitable to represent these branches as cylinders with the metal substrate along the central axis covered with a layer of active material. Proton diffusion inside the solid active material occurs simultaneously with the electron exchange between $Ni(OH)_2$ and NiOOH, which takes place in the radial direction.

The reactive sites in the hydrogen electrode are readily available to the reactants that reach the electrode and the hydrogen electrode has a much larger charge and discharge capability than the nickel electrode. Therefore, the hydrogen electrode is treated as a flat plate electrode.

Governing equations.—The governing equations for the porous nickel electrode and the separator were derived using the volume averaging technique over the appropriate free-stream equations.[17] The use of this technique results in some dependent variables to be averaged over the phases present in the porous electrode. As mentioned above, the gradients in the radial direction of the cell are neglected. Consequently, the model equations are written in one dimension, which is defined across the cell (x coordinate). For the nickel electrode we define a pseudo-second dimension in the active material (see Fig. 3).

The governing equations are written for seven dependent variables in the x direction, two dependent variables in the y direction for the nickel electrode, and three dependent variables that are a function of time only. In the following, the dependent variables that are averaged are enclosed by $\langle\ \rangle$, and the superscripts (l) and (g) denote that the variable is defined for the liquid or gas phase, respectively. The dependent variables in the x direction are: concentration of electrolyte, $\langle c_e\rangle^{(l)}$; concentration of dissolved oxygen, $\langle c_{O_2}\rangle^{(l)}$; concentration of dissolved hydrogen, $\langle c_{H_2}\rangle^{(l)}$; concentration of oxygen in the gas phase, $\langle c_{O_2}\rangle^{(g)}$; concentration of hydrogen in the gas phase, $\langle c_{H_2}\rangle^{(g)}$; current density in the electrolyte, $\langle \bar{i}^{(l)}\rangle$; and potential in the electrolyte, $\langle\phi\rangle^{(l)}$. The dependent variables in the y direction in the active material of the nickel electrode are the proton concentration, c_{H^+}, and the potential in the solid, $\phi^{(s)}$. The variables that are a function of time only are the concentrations of hydrogen and oxygen in the head space between the cell stack and the pressure vessel, $c_{H_2}^{ext}$ and $c_{O_2}^{ext}$, and the potential of the hydrogen electrode, ϕ_{H_2}. The governing equations are presented in the following paragraphs. The detailed derivation of the model equations is presented by De Vidts.[17]

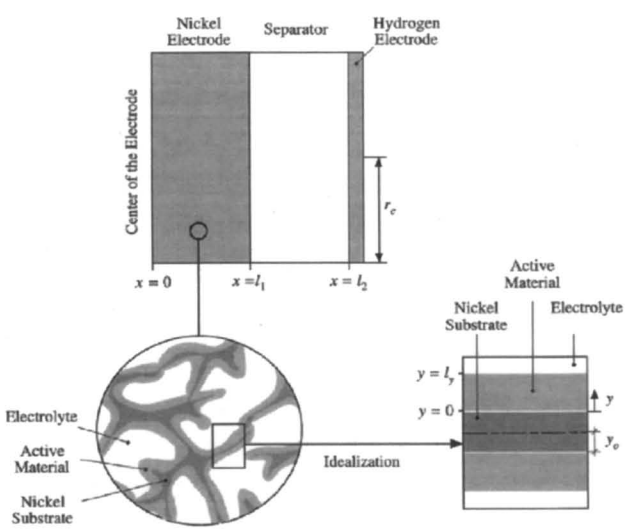

Fig. 3. Schematic diagram of the nickel/hydrogen cell showing the idealization of the nickel electrode and the coordinate system.

Nickel electrode.—Equations in the x direction

• Material balance of electrolyte ($0 < x < l_1$) is given by

$$\epsilon_{pos}^{(l)}\frac{\partial\langle c_e\rangle^{(l)}}{\partial t} - \left(\epsilon_{pos}^{(l)}\right)^b\frac{\partial}{\partial x}\left[\langle D_e\rangle^{(l)}\frac{\partial\langle c_e\rangle^{(l)}}{\partial x}\right] - \frac{t_-^3}{F}\frac{\partial\bar{i}^{(l)}}{\partial x} + \frac{a_{pos}^{(sl)}}{F}\left(\langle j_1\rangle^{(sl)} + \langle j_2\rangle^{(sl)} + \langle j_3\rangle^{(sl)}\right) = 0 \quad [6]$$

in which the concentration of electrolyte has been defined as

$$\langle c_e\rangle^{(l)} \equiv \frac{\langle c_+\rangle^{(l)}}{\nu_+} = \frac{\langle c_-\rangle^{(l)}}{\nu_-} \quad [7]$$

This definition for the electrolyte concentration allows us to satisfy the electroneutrality condition automatically, which for a binary electrolyte reads

$$z_+\langle c_+\rangle^{(l)} + z_-\langle c_-\rangle^{(l)} = 0 \quad [8]$$

Equation 6 indicates that the accumulation of electrolyte is the result of diffusion, migration, and the electrochemical reactions that involve hydroxyl ions (OH^-) at the active material/liquid interface.

• Material balance of dissolved hydrogen ($0 < x < l_1$)

The accumulation of dissolved hydrogen is the result of diffusion, the rate of reaction of reaction 3 taking place at the active material/liquid interface, and the flux of hydrogen from the liquid phase into the gas phase (gas pores). The flux of hydrogen from the liquid into the gas phase is assumed to be proportional to the difference between the equilibrium concentration and the actual concentration in the gas phase, as represented by the last term in Eq. 9

$$\epsilon_{pos}^{(l)}\frac{\partial\langle c_i\rangle^{(l)}}{\partial t} - \left(\epsilon_{pos}^{(l)}\right)^b D_i^{(l)}\frac{\partial^2\langle c_i\rangle^{(l)}}{\partial x^2} + \frac{a_{pos}^{(sl)}}{nF}\langle j_k\rangle^{(sl)} + a_{pos}^{(lg)}k_i^{(lg)}\left(\frac{\langle c_i\rangle^{(l)}}{K_{e,i}} - \langle c_i\rangle^{(g)}\right) = 0 \quad [9]$$

in which i = H_2, $k = 3$, and $n = 2$.

• Material balance of dissolved oxygen ($0 < x < l_1$) is analogous to that of hydrogen, with oxygen being involved in reaction 2 instead of reaction 3, that is, i = O_2, $k = 2$, $n = 4$ in Eq. 9.

• Material balance of hydrogen in the gas phase inside the cell stack ($0 < x < l_1$) includes a term for diffusion of a compressible gas, the flux of hydrogen from the liquid phase equivalent to that included in Eq. 9, and the flux of hydrogen from the cell stack into the head space. The flux into the head space is represented by the last term in Eq. 10 and we have assumed that is proportional to the

difference between the concentration of hydrogen in the gas pores and in the head space

$$\epsilon_{pos}^{(g)}\frac{\partial\langle c_i\rangle^{(g)}}{\partial t} - D_i^{(g)}\left(\epsilon_{pos}^{(g)}\right)^b\frac{\partial}{\partial x}\left[\frac{\partial^2\langle c_i\rangle^{(g)}}{\partial x} - \frac{\langle c_i\rangle^{(g)}}{\left(\langle c_i\rangle^{(g)}+\langle c_j\rangle^{(g)}\right)}\frac{\partial}{\partial x}\left(\langle c_i\rangle^{(g)}+\langle c_j\rangle^{(g)}\right)\right] - a_{pos}^{(lg)}k_i^{(lg)}\left(\frac{\langle c_i\rangle^{(l)}}{K_{e,i}} - \langle c_i\rangle^{(g)}\right) - \frac{2}{r_c}k_{pos}^{ext}RT\left(\langle c_i\rangle^{(g)} - c_i^{ext}\right) = 0 \quad [10]$$

in which i = H_2 and j = O_2.

• Material balance of oxygen in the gas phase inside the cell stack ($0 < x < l_1$) in the gas pores is analogous to that for hydrogen (Eq. 10) with i = O_2 and j = H_2.

• Modified Ohm's law in the electrolyte ($0 < x < l_1$): because the electrolyte is a concentrated solution of KOH we must include the effects of gradients in the electrolyte concentration when relating the current density and the potential in the liquid phase. That is, we must use a modified Ohm's law as described by Newman[15]

$$\bar{i}^{(l)} = -\langle\kappa\rangle^{(l)}\left(\epsilon_{pos}^{(l)}\right)^d\frac{\partial\langle\phi\rangle^{(l)}}{\partial x} - \frac{2RT}{F}\langle\kappa\rangle^{(l)}\left(\epsilon_{pos}^{(l)}\right)^d\left(1+\left\langle\frac{d\ln f_\pm}{d\ln c_e}\right\rangle^{(l)}\right)\left[1-\left(1+2\left\langle\frac{c_e}{c_o}\right\rangle^{(l)}\right)t_-^* + \frac{1}{2}\left\langle\frac{c_e}{c_o}\right\rangle^{(l)}\right]\frac{\partial\ln\langle c_e\rangle^{(l)}}{\partial x} \quad [11]$$

• Conservation of charge in the electrolyte ($0 < x < l_1$): we require that every portion of the electrode be neutral. That is, there must not be accumulation of charge in the solid, liquid, and gas phases. For the liquid phase, this results in that the change in current density must be equal to the current involved in all the electrochemical reactions taking place in the solid/liquid interface; as represented by

$$\frac{\partial\bar{i}^{(l)}}{\partial x} = a_{pos}^{(sl)}\left(\langle j_1\rangle^{(sl)} + \langle j_2\rangle^{(sl)} + \langle j_3\rangle^{(sl)}\right) \quad [12]$$

At the center of the nickel electrode ($x = 0$) the boundary conditions are

$$-\langle D\rangle^{(l)}\left(\epsilon_{pos}^{(l)}\right)^b\frac{\partial\langle c_e\rangle^{(l)}}{\partial x} = 0 \quad [13]$$

$$-D_i^{(l)}\left(\epsilon_{pos}^{(l)}\right)^b\frac{\partial\langle c_i\rangle^{(l)}}{\partial x} = 0 \quad i = H_2, O_2 \quad [14]$$

$$-D_i^{(g)}\left(\epsilon_{pos}^{(g)}\right)^b\left[\frac{\partial\langle c_i\rangle^{(g)}}{\partial x} - \frac{\langle c_i\rangle^{(g)}}{\left(\langle c_i\rangle^{(g)}+\langle c_j\rangle^{(g)}\right)}\frac{\partial}{\partial x}\left(\langle c_i\rangle^{(g)}+\langle c_j\rangle^{(g)}\right)\right] = 0 \quad [15]$$

with i = H_2 and j = O_2 for the hydrogen boundary condition and i = O_2 and j = H_2 for the oxygen boundary condition

$$\frac{\partial\langle\phi\rangle^{(l)}}{\partial x} = 0 \quad [16]$$

$$\frac{\partial\bar{i}^{(l)}}{\partial x} = a_{pos}^{(sl)}\left(\langle j_1\rangle^{(sl)} + \langle j_2\rangle^{(sl)} + \langle j_3\rangle^{(sl)}\right) \quad [17]$$

Equations 13-15 represent the condition of zero flux for all the species in the liquid and gas phases. Equation 16 indicates that all the current density leaves the electrolyte and enters the current collector and there is no accumulation of charge, as indicated by Eq. 17.

At the interface between the nickel electrode and the separator ($x = l_1$) the boundary conditions are

$$-\langle D^{(l)}\rangle\left(\epsilon_{pos}^{(l)}\right)^b\frac{\partial\langle c_e\rangle^{(l)}}{\partial x}\bigg|_{x=l_1^-} = -\langle D\rangle^{(l)}\left(\epsilon_{sep}^{(l)}\right)^b\frac{\partial\langle c_e\rangle^{(l)}}{\partial x}\bigg|_{x=l_1^+} \quad [18]$$

$$-D_i^{(l)}\left(\epsilon_{pos}^{(l)}\right)^b\frac{\partial\langle c_i\rangle^{(l)}}{\partial x}\bigg|_{x=l_1^-} = -\langle D\rangle_i^{(l)}\left(\epsilon_{sep}^{(l)}\right)^b\frac{\partial\langle c_i\rangle^{(l)}}{\partial x}\bigg|_{x=l_1^+} \quad i = H_2, O_2 \quad [19]$$

$$-D_i^{(g)}\left(\epsilon_{pos}^{(g)}\right)^b\left[\frac{\partial\langle c_i\rangle^{(g)}}{\partial x} - \frac{\langle c_i\rangle^{(g)}}{\left(\langle c_i\rangle^{(g)}+\langle c_j\rangle^{(g)}\right)}\frac{\partial}{\partial x}\left(\langle c_i\rangle^{(g)}-\langle c_j\rangle^{(g)}\right)\right]_{x=l_1^-} = -D_i^{(g)}\left(\epsilon_{sep}^{(g)}\right)^b\left[\frac{\partial\langle c_i\rangle^{(g)}}{\partial x} - \frac{\langle c_i\rangle^{(g)}}{\left(\langle c_i\rangle^{(g)}+\langle c_j\rangle^{(g)}\right)}\frac{\partial}{\partial x}\left(\langle c_i\rangle^{(g)}+\langle c_j\rangle^{(g)}\right)\right]\bigg|_{x=l_1^+} \quad [20]$$

with i = H_2 and j = O_2 for the hydrogen boundary condition and i = O_2 and j = H_2 for the oxygen boundary condition

$$-\langle\kappa\rangle^{(l)}\left(\epsilon_{pos}^{(l)}\right)^d\frac{\partial\langle\phi\rangle^{(l)}}{\partial x}\bigg|_{x=l_1^-} = -\langle\kappa\rangle^{(l)}\left(\epsilon_{sep}^{(l)}\right)^d\frac{\partial\langle\phi\rangle^{(l)}}{\partial x}\bigg|_{x=l_1^+} \quad [21]$$

$$\bar{i}^{(l)} = i_{cell} \quad [22]$$

Equations 18-20 indicate that in the liquid and gas phases the flux of species leaving the nickel electrode is equal to that entering the separator. The current density in the liquid phase leaving the nickel electrode also must be equal to that entering the separator, as indicated by Eq. 21. In the separator all the applied current travels through the liquid phase because the solid material is an electrical insulator; thus, the current density is equal to the current applied to the cell, as indicated by Eq. 22.

Equations in the y direction

• Proton diffusion for $0 < y < l_y$: the proton diffusion inside the solid active material occurs simultaneously with the electron exchange between $Ni(OH)_2$ and NiOOH, which takes place in the radial direction. Assuming that there are no gradients in the angular direction, the equation of continuity for the proton in cylindrical coordinates takes the form

$$\frac{\partial c_{H^+}}{\partial t} = \frac{1}{(y+y_o)}\frac{\partial}{\partial y}\left(D_{H^+}^{(s)}(y+y_o)\frac{\partial c_{H^+}}{\partial y}\right) \quad [23]$$

where y is the radial coordinate defined from the nickel substrate to the active material/electrolyte interface, as shown in Fig. 3.

• Conservation of charge: no accumulation of charge in the solid active material means that the divergence of the current density in the solid must be equal to zero; which in cylindrical coordinates reads

$$\frac{1}{(y+y_o)}\frac{\partial}{\partial y}\left((y+y_o)\sigma^{(s)}\frac{\partial\phi^{(s)}}{\partial y}\right)=0 \qquad [24]$$

The diffusion coefficient of protons and the conductivity of the active material are functions of the state of charge (content of protons). The expressions for these quantities are included below.

The boundary conditions at the interface of the electrolyte and the active material ($y = l_y$) are

$$-D^{(s)}_{H^+}\frac{\partial c_{H^+}}{\partial y}\bigg|_{y=l_y}=\frac{\langle j_1\rangle^{(sl)}}{F} \qquad [25]$$

$$-\sigma^{(s)}\frac{\partial\phi^{(s)}}{\partial y}\bigg|_{y=l_y}=\left(\langle j_1\rangle^{(sl)}+\langle j_2\rangle^{(sl)}+\langle j_3\rangle^{(sl)}\right) \qquad [26]$$

Equation 25 indicates that the flux of protons is equal to what is being produced by reaction 1. Equation 26 indicates that the current density in the solid at the solid/liquid interface is equal to the sum of the partial currents due to all the electrochemical reactions taking place at that interface.

The boundary conditions at the interface of the active material and the nickel substrate ($y = 0$) are

$$-D^{(s)}_{H^+}\frac{\partial c_{H^+}}{\partial y}\bigg|_{y=l_y}=0 \qquad [27]$$

$$\phi^{(s)}\big|_{y=l_y}=\phi_{sub} \qquad [28]$$

Equations 27 and 28 indicate that protons do not enter the nickel substrate and that the potential in the active material is the same as that in the nickel substrate.

Separator.—In the separator we have equations in the x direction only, because there are no reactions taking place and the solid phase is an electrical insulator. Thus, the governing equations are analogous to Eq. 6 through 12 for the nickel electrode but with no reactions and with $l_1 < x < l_2$. Also, the current density in the liquid is equal to the current density applied to the cell because the solid phase in the separator is an electrical insulator.

Hydrogen electrode.—As was mentioned before, the hydrogen electrode is treated as a flat plate electrode. Therefore, the governing equations for this electrode become the boundary conditions for the separator at $x = l_2$.

The current that reaches the hydrogen electrode is used in the hydrogen and oxygen reactions (reactions 4 and 5), thus

$$-i_{cell}=a^{(sl)}_{neg}(j_4+j_5) \qquad [29]$$

where $a^{(sl)}_{neg}$ is the active surface area per unit of cross-sectional area of electrode in cm^2/cm^2. Equation 29 is the governing equation for the potential in the hydrogen electrode, ϕ_{H_2}, which is involved in the kinetic expressions for reactions 4 and 5 (j_4 and j_5). The kinetic expressions for all five reactions are included in the next section.

The current density in the liquid phase is equal to the current applied to the cell and it is also equal to the flux of hydroxyl ions; that is

$$\bar{i}^{(l)}=i_{cell} \qquad [30]$$

$$-\left(\epsilon^{(l)}_{pos}\right)^b\langle D\rangle^{(l)}\frac{\partial\langle c_e\rangle^{(l)}}{\partial x}+\frac{t^*_-}{F}\bar{i}^{(l)}=i_{cell} \qquad [31]$$

On the back of the hydrogen electrode there is a gas screen to facilitate the mass transfer of hydrogen and oxygen between the hydrogen electrode and the gas contained in the head space between the cell stack and the pressure vessel (external gas phase). The Teflon backing of the electrode is permeable to gas but not to liquid. Therefore, there is flux of gaseous species into or out of the hydrogen electrode without loss of electrolytic solution. We can assume that the external gas is in contact with the liquid phase because the external gas is in contact with the back of the hydrogen electrode through the gas screen and it can penetrate the Teflon backing. Therefore, the fluxes of dissolved hydrogen and oxygen are equal to the rate of reaction of reactions 4 and 5 plus what is exchanged with the external gas phase if the liquid and external gas phase are not in equilibrium

$$-D^{(l)}_i\left(\epsilon^{(l)}_{sep}\right)^b\frac{\partial\langle c_i\rangle^{(l)}}{\partial x}=a^{(sl)}_{neg}\frac{j_k}{nF}+k^{(lg,ext)}_i\left(\frac{\langle c_i\rangle^{(l)}}{K_{e,i}}-c^{ext}_i\right) \qquad [32]$$

with i = H_2, $k = 4$, and $n = 2$ for the hydrogen flux and i = O_2, $k = 5$, and $n = 4$ for the oxygen flux.

The fluxes for hydrogen and oxygen gas are caused by the difference between the internal and external concentrations of each species

$$-D^{(g)}_i\left(\epsilon^{(g)}_{sep}\right)^b\left[\frac{\partial\langle c_i\rangle^{(g)}}{\partial x}-\frac{\langle c_i\rangle^{(g)}}{\langle c_i\rangle^{(g)}+\langle c_j\rangle^{(g)}}\frac{\partial}{\partial x}\left(\langle c_i\rangle^{(g)}+\langle c_j\rangle^{(g)}\right)\right]_{x=l_2}$$

$$=k^{ext}_{tef}RT\left(\langle c_i\rangle^{(g)}-c^{ext}_i\right) \qquad [33]$$

with i = H_2 and j = O_2 for the hydrogen flux and i = O_2 and j = H_2 for the oxygen flux .

Material balance of hydrogen and oxygen contained in the head space.—The change in the number of moles of hydrogen and oxygen in the external gas phase is equal to the integral of the fluxes through the surface of the cell stack and the back of the hydrogen electrode

$$\frac{dn^{ext}_i}{dt}=2\pi r_c\int_0^{l_1}k^{ext}_{pos}RT\left(\langle c_i\rangle^{(g)}-c^{ext}_i\right)dx$$

$$+2\pi r_c\int_{l_1}^{l_2}k^{ext}_{sep}RT\left(\langle c_i\rangle^{(g)}-c^{ext}_i\right)dx+\pi r_c^2k^{ext}_{tef}RT\left(\langle c_i\rangle^{(g)}-c^{ext}_i\right)$$

$$+\pi r_c^2k^{(lg,ext)}_i\left(\frac{\langle c_i\rangle^{(l)}}{K_{e,i}}-c^{ext}_i\right) \qquad [34]$$

with i = H_2, O_2. We can divide Eq. 34 by the volume of the head space between the cell stack and the pressure vessel, V^{ext}. This external volume is a design parameter and does not change with time; thus

$$\frac{dc^{ext}_i}{dt}=\frac{2\pi r_c}{V^{ext}}\int_0^{l_1}k^{ext}_{pos}RT\left(\langle c_i\rangle^{(g)}-c^{ext}_i\right)dx+\frac{2\pi r_c}{V^{ext}}$$

$$\int_{l_1}^{l_2}k^{ext}_{sep}RT\left(\langle c_i\rangle^{(g)}-c^{ext}_i\right)dx+\frac{\pi r_c^2k^{ext}_{tef}RT}{V^{ext}}\left(\langle c_i\rangle^{(g)}-c^{ext}_i\right)$$

$$+\frac{\pi r_c^2k^{(lg,ext)}_i}{V^{ext}}\left(\frac{\langle c_i\rangle^{(l)}}{K_{e,i}}-c^{ext}_i\right) \qquad [35]$$

with i = H_2, O_2. Equation 35 is the governing equation for the concentration of hydrogen and oxygen gas in the external gas phase.

Electrode kinetics.—The Butler-Volmer equation is used to express the rates of reaction for the five reactions that take place in this cell (Eq. 1-5). We assume that the orders of reaction correspond to the stoichiometric coefficients of each reaction. The equilibrium potentials are expressed

with respect to a Hg/HgO reference electrode, which is at the same conditions as the working electrode.

Reaction 1

$$\langle j_1\rangle^{(sl)} = j_{o,1,ref}\left\{\left(\frac{\langle c_e\rangle^{(l)}}{\langle c_{e,ref}\rangle^{(l)}}\right)\left(\frac{c_{H^+}}{c_{H^+,ref}}\right)_{y=l_y} \exp\left(\frac{\alpha_{a1}F}{RT}\eta_1\right) - \left(\frac{c_{H^+,max} - c_{H^+}}{c_{H^+,max} - c_{H^+,ref}}\right)_{y=l_y} \exp\left(\frac{-\alpha_{c1}F}{RT}\eta_1\right)\right\} \quad [36]$$

Reaction 2

$$\langle j_2\rangle^{(sl)} = j_{o2,ref}\left\{\left(\frac{\langle c_e\rangle^{(l)}}{\langle c_{e,ref}\rangle^{(l)}}\right)^2 \exp\left(\frac{\alpha_{a2}F}{RT}\eta_2\right) - \left(\frac{\langle c_{O_2}\rangle^{(l)}}{\langle c_{O_2,ref}\rangle^{(l)}}\right)^{1/2} \exp\left(\frac{-\alpha_{c2}F}{RT}\eta_2\right)\right\} \quad [37]$$

Reaction 3

$$\langle j_3\rangle^{(sl)} = j_{o3,ref}\left\{\left(\frac{\langle c_e\rangle^{(l)}}{\langle c_{e,ref}\rangle^{(l)}}\right)^2 \left(\frac{\langle c_{H_2}\rangle^{(l)}}{\langle c_{H_2,ref}\rangle^{(l)}}\right) \exp\left(\frac{\alpha_{a3}F}{RT}\eta_3\right) - \exp\left(\frac{-\alpha_{c3}F}{RT}\eta_3\right)\right\} \quad [38]$$

Reaction 4

$$j_4 = j_{04,ref}\left\{\left(\frac{\langle c_e\rangle^{(l)}}{\langle c_{e,ref}\rangle^{(l)}}\right)^2 \left(\frac{\langle c_{H_2}\rangle^{(l)}}{\langle c_{H_2,ref}\rangle^{(l)}}\right) \exp\left(\frac{\alpha_{a4}F}{RT}\eta_4\right) - \exp\left(\frac{-\alpha_{c4}F}{RT}\eta_4\right)\right\} \quad [39]$$

Reaction 5

$$j_5 = j_{05,ref}\left\{\left(\frac{\langle c_e\rangle^{(l)}}{\langle c_{e,ref}\rangle^{(l)}}\right)^2 \exp\left(\frac{\alpha_{a5}F}{RT}\eta_5\right) - \left(\frac{\langle c_{O_2}\rangle^{(l)}}{\langle c_{O_2,ref}\rangle^{(l)}}\right)^{1/2} \exp\left(\frac{-\alpha_{c5}F}{RT}\eta_5\right)\right\} \quad [40]$$

The overpotential for reactions 1, 2, and 3 is defined as

$$\eta_k = \phi^{(s)}\big|_{y=l_y} - \langle\phi\rangle^{(l)} - \phi_{eqk,ref} \quad k = 1, 2, 3 \quad [41]$$

whereas for reactions 4 and 5

$$\eta_k = \phi_{H_2} - \langle\phi^{(l)}\rangle\big|_{x=l_2} - \phi_{eqk,ref} \quad k = 4,5 \quad [42]$$

The equilibrium potential for reaction 1 evaluated at reference conditions is given by

$$\phi_{eqk,ref} = 0.427 - \frac{RT}{F}\ln\left(\frac{c_{H^+,ref}}{c_{H^+,max} - c_{H^+,ref}}\right) \quad [43]$$

The equilibrium potentials for reactions 2 and 5 evaluated at reference conditions are given by

$$\phi_{eqk,ref} = 0.3027 + \frac{RT}{4F}\ln\left(p_{O_2,ref}\right) \quad k = 2,5 \quad [44]$$

Finally, the equilibrium potentials for reactions 3 and 4 evaluated at reference conditions are given by

$$\phi_{eqk,ref} = -0.9263 - \frac{RT}{2F}\ln\left(p_{H_2,ref}\right) \quad k = 3,4 \quad [45]$$

Initial conditions.—The initial conditions to start a discharge and charge simulation are given in Table I. Alternatively, the final solution of one process can be used as the initial conditions for the following process.

Model parameters.—The value for the parameters involved in the equations are listed in Table II. The relations presented in Eq. 46-50 were used to estimate some physical parameters of the nickel electrode presented in Table II. These equations were presented in Mao *et al.*[8]

Table I. Initial conditions for discharge and charge.

	Discharge	Charge
$\langle c_e\rangle^{(l)}$	5.8×10^{-3} mol/cm^3	5.8×10^{-3} mol/cm^3
c_{H^+}	0.3668×10^{-5} mol/cm^3 (fully charged nickel electrode)	0.03668 mol/cm^3 (fully discharged nickel electrode)
$p^0_{O_2}$	0.04 atm	10^{-6} atm
p^0_{H2}	52.2 atm for $i_{cell} = -16.25$ mA/cm^2, 52.3 atm for $i_{cell} = -32.5$ mA/cm^2, 52.1 atm for $i_{cell} = -65$ mA/cm^2	49 atm for $i_{cell} = 16.25$ mA/cm^2, 49 atm for $i_{cell} = 32.5$ mA/cm^2, 48.3 atm for $i_{cell} = 65$ mA/cm^2
$\langle c_{H_2}\rangle^{(g)}$		$\frac{p^0_{H_2}}{RT}$
$\langle c_{O_2}\rangle^{(g)}$		$\frac{p^0_{O_2}}{RT}$
$\langle c_{H_2}\rangle^{(l)}$		$K_{e,H_2}\langle c_{H_2}\rangle^{(g)}$
$\langle c_{O_2}\rangle^{(l)}$		$K_{e,O_2}\langle c_{O_2}\rangle^{(g)}$
$c^{ext}_{H_2}$		$\frac{p^0_{H_2}}{RT}$
$c^{ext}_{O_2}$		$\frac{p^0_{O_2}}{RT}$

Table II. Model parameters used in the simulations.

Parameter	Value	Source
a_o	2000 cm^2/cm^3	
a_{pos}	4138 cm^2/cm^3	Eq. 50
$a_{pos}^{(sl)}$	4138 cm^2/cm^3	
$a_{neg}^{(sl)}$	25 cm^2/cm^2	
$a_{pos}^{(lg)}$	10^4 cm^2/cm^3	
$a_{sep}^{(lg)}$	10^4 cm^2/cm^3	
b	1.5	Ref. 22
$\langle c_{e,ref}\rangle^{(l)}$	5.8×10^{-3} mol/cm^3	
$c_{H^+,max}$	0.03667 mol/cm^3	Eq. 46
$c_{H^+,ref}$	$0.5c_{H^+,max}$	
$\langle c_{H_2,ref}\rangle^{(l)}$	1.461×10^{-6} mol/cm^3	Ref. 23
$\langle c_{O_2,ref}\rangle^{(l)}$	1.529×10^{-11} mol/cm^3	Ref. 23
d	1.5	Ref. 22
$D_{H_2}^{(g)}$	0.697 cm^2/s	Ref. 24
$D_{O_2}^{(g)}$	0.697 cm^2/s	Ref. 24
$D_{H_2}^{(l)}$	1.53×10^{-5} cm^2/s	Ref. 25
$D_{O_2}^{(l)}$	6×10^{-6} cm^2/s	Ref. 26
F	96,487 C/eq	
$j_{o1,ref}$	2×10^{-4} A/cm^2	
$j_{o2,ref}$	10^{-10} A/cm^2	Ref. 27
$j_{o3,ref}$	5×10^{-18} A/cm^2	
$j_{o4,ref}$	3.5×10^{-4} A/cm^2	Ref. 28
$j_{o5,ref}$	10^{-10} A/cm^2	
K_{e,H_2}	7.153×10^{-4}	Ref. 23
K_{e,O_2}	7.486×10^{-4}	Ref. 23
k_{pos}^{ext}	25 mol/atm cm^2 s	Ref. 29
k_{sep}^{ext}	25 mol/atm cm^2 s	Ref. 29
k_{tef}^{ext}	25 mol/atm cm^2 s	Ref. 29
$k_{H_2}^{(lg)}$	3×10^{-4} cm/s	Ref. 24
$k_{O_2}^{(lg)}$	2×10^{-4} cm/s	Ref. 24
$k_{H_2}^{(lg,ext)}$	3×10^{-4} cm/s	Ref. 24
$k_{O_2}^{(lg,ext)}$	2×10^{-4} cm/s	Ref. 24
l_1	0.072 cm	
l_2	0.114 cm	
l_y	1.2×10^{-4} cm	Eq. 49
M_{KOH}	56 g/gmol	
$M_{Ni(OH)_2}$	92.7 g/gmol	
$p_{H_2,ref}$	50 atm	
$p_{O_2,ref}$	5×10^{-4} atm	
Q_{max}	117 C/cm^2 (32.5 mAh/cm^2)	
R	8.3143 J/mol K	
r_c	2.5 cm	
T	298.15 K	
t_-^3	0.78	Ref. 27
V^{ext}	87.7 cm^3	
α_{a1}	0.5	
α_{c1}	0.5	
α_{a2}	1.25	Ref. 27
α_{c2}	0.75	
α_{a3}	0.5	Ref. 28
α_{c3}	0.5	
α_{a4}	0.5	Ref. 30
α_{c4}	0.5	
α_{a5}	1.75	
α_{c5}	0.25	
y_o	1.4×10^{-4} cm	Eq. 48
ϵ_{pos}	0.4	Eq. 47
$\epsilon_{o,pos}$	0.86	Ref. 29
$\epsilon_{pos}^{(g)}$	0.04	
$\epsilon_{sep}^{(g)}$	0.085	
$\epsilon_{pos}^{(l)}$	0.36	
$\epsilon_{sep}^{(l)}$	0.765	
ϕ_{sub}	0.427 V	
$\rho_{Ni(OH)_2}$	3.4 g/cm^3	Ref. 8
ρ_o	1 g/cm^3	

The parameters that have no source are either assumed values or design parameters.

and were derived assuming that the porosity for the nickel substrate, $\epsilon_{o,pos}$, and the theoretical charge of the nickel electrode, Q_{max}, are known, and that the nickel substrate consists of a collection of cylinders covered with a layer of active material (see Fig. 3).

Maximum proton concentration

$$c_{H^+,max} = \frac{\rho_{Ni(OH)_2}}{M_{Ni(OH)_2}} \quad [46]$$

Porosity of the nickel electrode

$$\epsilon_{pos} = \epsilon_{o,pos} - \frac{Q_{max}}{Fc_{H^+,max}l_1} \quad [47]$$

Radius of the nickel substrate in cylindrical shape

$$y_o = \frac{2(1 - \epsilon_{o,pos})}{a_o} \quad [48]$$

Thickness of the active material

$$l_y = y_o\sqrt{1 + \frac{2(\epsilon_{o,pos} - \epsilon_{pos})}{y_o a_o}} - y_o \quad [49]$$

Specific active surface area of the nickel electrode

$$a_{pos} = a_o\sqrt{\frac{1 - \epsilon_{pos}}{1 - \epsilon_{o,pos}}} \quad [50]$$

The properties D, κ, c_e/c_o, and $\ln f_\pm$ are functions of the electrolyte concentration, c_e. Correlations for these properties were obtained by fitting polynomials on c_e to experimental data for each property found in the literature.

The expression for the diffusion coefficient of the electrolyte (KOH) was obtained using experimental data reported for the integral diffusion coefficient at 25°C for electrolyte concentrations in the range 0.103 to 13.719 × 10^{-3} mol/cm^3 [18]

$$D_{integ} = \exp(-10.467 - 8.1607c_e^{1/2} + 286.2c_e - 2539.8c_e^{3/2} + 7207.5c_e^2) \quad [51]$$

The regression had an average relative error of 0.36%. The differential diffusion coefficient, D, is given by

$$D = D_{integ}\left(c_e\frac{dD_{integ}}{dc_e} + 1\right)$$

$$= D_{integ}\left(1.0 - 4.0804c_e^{1/2} + 286.2c_e - 3809.7c_e^{3/2} + 14415c_e^2\right) \quad [52]$$

The following expression was obtained for the specific conductivity of the free-electrolyte, κ, using experimental data for the equivalent conductance at 25°C for electrolyte concentrations in the range 0.06081 to 10.611 × 10^{-3} mol/cm^3 [18]

$$\kappa = c_e \exp\left(5.5657 - 6.1538c_e^{1/2} + 13.408c_e - 1075.8c_e^{3/2}\right) \quad [53]$$

The regression had an average relative error of 0.16%.

The ratio of electrolyte concentration to water concentration, c_e/c_o, was obtained using experimental data for the density of the electrolyte at 25°C [18]

$$\frac{c_e}{c_o} = -1.4041 \times 10^{-4} + 18.2c_e + 100.25c_e^2 + 23811c_e^{3/2} \quad [54]$$

The experimental data used for the regression is for electrolyte concentrations in the range 0.3617 to 13.449 × 10^{-3} mol/cm^3. The regression had an average relative error of 0.53%.

The mean molar activity coefficient of the electrolyte is given by

$$f_{\pm} = \gamma_{\pm}\left(\frac{\rho_{H_2O}}{\rho - M_{KOH}c_e}\right) \quad [55]$$

Using experimental data for the molal activity coefficient, $\gamma_{\pm}$, and density, ρ, of the electrolyte solution at 25°C [18] we obtained the following expressions

$$\ln \gamma_{\pm} = \frac{-1.1813\sqrt{m}}{1 + \sqrt{m}} + 0.3848m - 0.03205m^{3/2} \quad [56]$$

$$\rho = 1.0002 + 45.726c_e - 601.63c_e^2 \quad [57]$$

in which the molality is given by

$$m = \frac{1000\, c_e}{\rho - M_{KOH}c_e} \quad [58]$$

For the model equations we need the volume averaged properties $\langle D\rangle^{(l)}$, $\langle \kappa\rangle^{(l)}$, $\langle c_e/c_o\rangle^{(l)}$, and $\langle \ln f_{\pm}\rangle^{(l)}$. We assume that the volume averaged of each property is approximately equal to the property evaluated at the volume averaged concentration of electrolyte; that is

$$\langle D\rangle^{(l)} = D\left(\langle c_e\rangle^{(l)}\right) \quad [59]$$

$$\langle \kappa\rangle^{(l)} = \kappa\left(\langle c_e\rangle^{(l)}\right) \quad [60]$$

$$\langle c_e/c_o\rangle^{(l)} = c_e/c_o\left(\langle c_e\rangle^{(l)}\right) \quad [61]$$

$$\langle \ln f_{\pm}\rangle^{(l)} = \ln f_{\pm}\left(\langle c_e\rangle^{(l)}\right) \quad [62]$$

The diffusion coefficient of protons in the active material of the nickel electrode has been found to be a function of the proton concentration[19]

$$D^{(s)}_{H^+} = 3.4 \times 10^{-8}\left[1 - \frac{c_{H^+}}{c_{H^+,max}} + \left(\frac{6.4 \times 10^{-11}}{3.4 \times 10^{-8}}\right)^{1/2}\left(\frac{c_{H^+}}{c_{H^+,max}}\right)\right]^2 \quad [63]$$

The conductivity of the active material, $\sigma^{(s)}$, also is considered a function of the proton concentration[2]

$$\sigma^{(s)} = 0.1185 \exp\left[-8.459\left(\frac{c_{H^+}}{c_{H^+,max}}\right)^4\right] \quad [64]$$

Method of solution.—The model consists of a set of partial differential equations in time, t, and two space coordinates, x and y. The model equations are Eq. 6, 9-33, and 35. The model is solved for the initial conditions shown in Table I and parameter values listed in Table II and Eq. 46-64.

The solution of the model equations is achieved by using the numerical method of lines.[20,21] This method consists in using finite differences to represent the derivatives in the spatial direction, transforming the original set of partial differential equations into a system of mixed-differential and algebraic equations with the independent variable being time, t. The method was implemented in Fortran 77 and uses the software DASSL, which is a sophisticated differential-algebraic equation solver that implements adaptive time-stepping and error control.[20] The simulations presented here were obtained using a Power Macintosh 7500/100. A typical discharge simulation takes about 10 min.

Experimental

A schematic diagram of the nickel/hydrogen cell used in the experiments is shown in Fig. 4. The cell consists of a nickel electrode, a two-layer polyethylene separator, a hydrogen electrode, and a gas screen, which are held together by two perforated plastic plates. The cell is contained in a stainless steel vessel with a pool of electrolyte (26% wt KOH) in the bottom. A Hg/HgO reference electrode is placed in the vessel so that it touches the separator as it enters the pool of electrolyte, as shown in Fig. 4. A needle pressure gauge is connected to the vessel to monitor the pressure of the cell. The cap of the vessel has three stainless steel leads that go into the vessel and are connected to the nickel, hydrogen, and reference electrodes. The leads are insulated from the cap by ceramic tubes. The nickel electrode (positive) consists of a sintered porous nickel plaque that is electrochemically impregnated with nickel hydroxide active material. The hydrogen electrode (negative) consists of a Teflon-bonded platinum black catalyst supported on a fine mesh nickel screen with Teflon backing. The properties of the cell components are presented in Table III. The operation of the cell was performed and controlled through a potentiostat/galvanostat EG&G PAR Model 273A.

The capacity of the nickel electrode was determined by two methods: dissolving the active material in acetic acid and by discharging the nickel electrode at 15, 6, and 3 mA/cm^2. The value of 32.5 mAh/cm^2 is an average of the results obtained from the chemical method. The results from the discharge experiments gave an average of 32.3 mAh/cm^2. The results from the experiments done dissolving the active material also were used to estimate the porosity of the nickel substrate. The estimated porosity was 0.86.

Prior to the experiments, the cell was precycled three or four times. Each cycle consists of 1.0 h of charging at 32.5 mA/cm^2 followed by discharge at 16.25 mA/cm^2 to a cell voltage of 0.5 V. After the precycling of the cell, the collection of data started. The charge operations always started after the last discharge at C/2 rate of the precycling. The discharge operation started after charging the cell at 1C rate for 1 h.

Results and Discussion

The model formulated in the previous section is used to simulate the dynamic behavior of a nickel/hydrogen cell during charge and discharge. One can examine the effects of various design and operating parameters, such as elec-

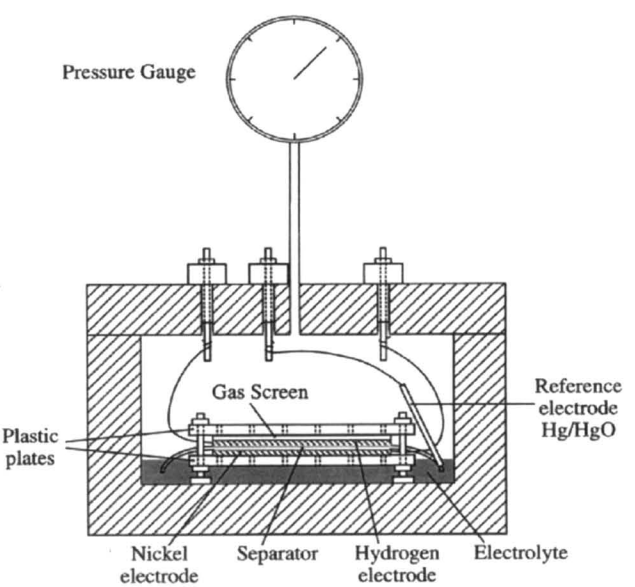

Fig. 4. Schematic diagram of the experimental apparatus.

Table III. Physical properties of the cell components.

Cell component	Property	Value
Nickel electrode	Geometrical area	20 cm^2
	Thickness	0.072 cm
	Capacity	32.5 mAh/cm^2
Separator	Thickness	0.04 cm
Hydrogen electrode	Geometrical area	20 cm^2
	Hydrogen pressure	700 psig (precharge pressure)
Electrolyte	Composition	5.8 *M* or 26% wt KOH aqueous solution
Head space inside the vessel	Volume	87.7 cm^3

trode plate thickness, separator thickness, active material loading, and charge/discharge rate on the cell performance. In the simulations presented in this section we use quantities that need to be defined. The cell voltage is defined as the difference between the potential of the nickel substrate at the positive electrode, ϕ_{sub}, and that of the negative electrode, ϕ_{H_2}. The state of charge of the cell is considered to be that of the nickel (positive) electrode, because the nickel/hydrogen cell is positive limited, that is, the nickel electrode has less charge than the negative electrode. The state of charge, *SOC*, and state of discharge, *SOD*, are defined as

$$SOC = \frac{Q}{Q_{max}} \quad [65]$$

$$SOD = 1 - \frac{Q}{Q_{max}} \quad [66]$$

where Q is the amount of charge (amount of NiOOH) present in the nickel electrode and is given by

$$Q = \frac{(1 - \epsilon_{pos})F}{\pi(y_o + l_y)^2} \int_{x=0}^{x=l_1} \int_{y=0}^{y=l_y} 2\pi(y + y_o)\left(c_{H^+,max} - c_{H^+}\right)dydx \quad [67]$$

The values of the model parameters used for the simulations are given in Table II.

Simulations of the discharge operation.—A comparison of the model predicted voltage-time and pressure-time behavior to experimental data of a nickel/hydrogen cell discharged at constant current is presented in Fig. 5 and 6. The three discharge current densities are 65.0, 32.5, and 16.25 mA/cm^2, which correspond to discharge rates of 2C, C, and C/2, respectively. The simulated curves agree well with the experimental data. The cell voltage exhibits the general behavior of the experimental curves but there are some quantitative deviations specially at the beginning of discharge where the simulated curves are flatter than the experimental curves. Also, the sharp fall of the cell voltage at the end of the first plateau seems to happen earlier in the experimental curves than in the simulated ones. These two deviations may be caused by inappropriate values for the kinetic parameters of the various reactions and the diffusion coefficient of protons in the nickel electrode. The simulated cell pressure shows an excellent agreement with the experimental data, as shown in Fig. 6, which may indicate that the hydrogen electrode is well represented in the model.

During discharge, the model prediction indicates that the cell voltage drops quickly from the open-circuit potential to a certain value at the early stages of discharge, then decays very slowly during the main course of discharge forming a discharge plateau and falls off by the end of discharge. At about 0.6-0.8 V, depending on the discharge rate, the voltage forms a second plateau much narrower than the first plateau. Finally, on the end of discharge the voltage falls off again. During discharge, the cell pressure decreases almost linearly with time except at the end of discharge, as shown in Fig. 6.

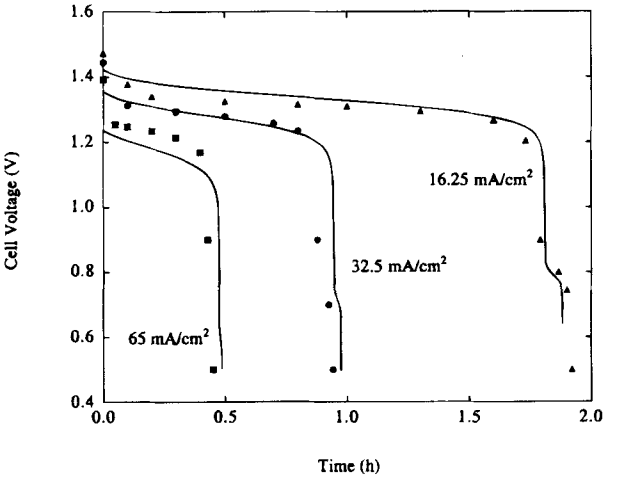

Fig. 5. Comparison of simulated and experimental cell voltage during discharge at various rates of discharge. The continuous lines are the simulated curves and the symbols are the experimental data.

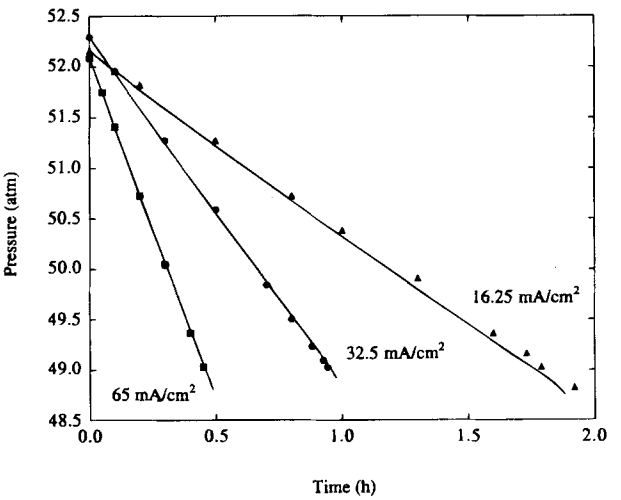

Fig. 6. Comparison of simulated and experimental cell pressure during discharge at various rates of discharge.

Figure 7 shows the predicted current densities of each reaction during discharge at -16.25 mA/cm^2 (C/2). At the beginning of discharge the current density of the main reaction (reaction 1) is greater, that is, more negative, than the set discharge rate, because the overpotential of the positive electrode is higher than the equilibrium potential of the oxygen reaction (reaction 2) and hydrogen reaction (reaction 3). Therefore, oxygen evolution and hydrogen oxidation occur in the positive electrode. The current density generated by these reactions is used by the main nickel reaction (reaction 1) in addition to the applied current density. Thus, the active material is being discharged by the applied current density and the current density of reactions 2 and 3; the latter is called self-discharge of the nickel electrode. As the discharge proceeds the potential of the nickel electrode decreases and the oxygen and hydrogen reactions tend to disappear. By the end of discharge, the potential of the electrode reaches values low enough for the oxygen reduction to take place, which coincides with the formation of the second plateau shown in Fig. 5.

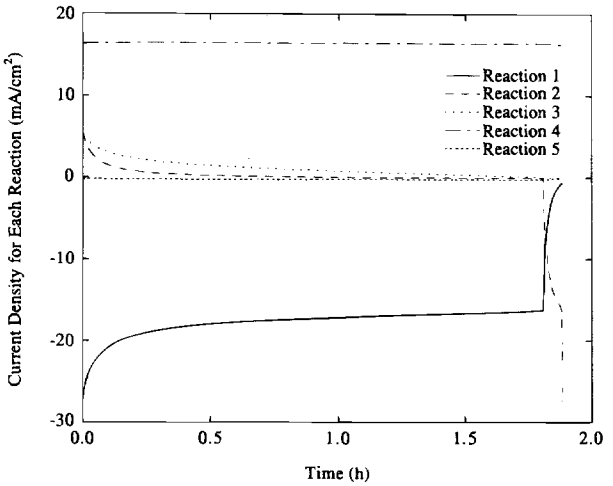

Fig. 7. Simulated current densities of each reaction in the cell for a discharge rate of −16.25 mA/cm² (C/2).

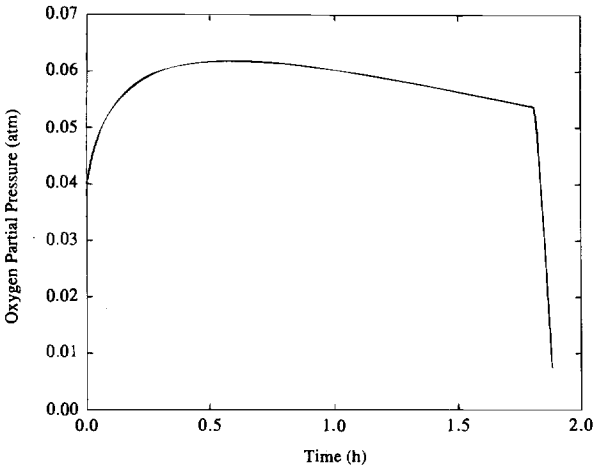

Fig. 9. Simulated oxygen partial pressure in the head space between the cell stack and the pressure vessel for a discharge rate of −16.25 mA/cm² (C/2).

During this second discharge plateau, the applied current switches from being used by the main nickel reaction (reaction 1) to being used by the oxygen reaction (reaction 2). In the negative electrode, the applied current is used on the hydrogen oxidation reaction (reaction 4) and the oxygen reaction is negligible.

Figure 8 shows the hydrogen pressure in the head space of the cell during discharge at a constant current of −16.25 mA/cm². The cell has a high content of hydrogen before discharge and the hydrogen is consumed by reaction 4 as the discharge proceeds. The simulation shows that the decrease on hydrogen pressure is practically linear with time. Figure 9 presents the oxygen pressure in the head space against time. Oxygen is produced by reaction 2 at the beginning of discharge. As the discharge proceeds, the oxygen evolution tends to disappear. By the end of discharge, reaction 2 occurs in the direction of oxygen reduction and the oxygen pressure drops sharply.

The hydrogen content in the gas phase inside the pores of the cell components, decreases with time following the behavior to the hydrogen in the head space (results not shown). The concentration in the internal gas phase does not change with position (x direction). This suggests that the mass-transfer resistance in the gas pores is negligible for the parameter values used in this simulation. The hydrogen concentration in the liquid follows the overall behavior of hydrogen in gas phase except near the hydrogen (negative) electrode where reaction 4 is taking place; the gradient in concentration caused by the consumption of hydrogen at that point.

The oxygen concentration in the liquid and gas phases follows the behavior of the oxygen pressure and increases over most of the discharge and it drops sharply at the end of discharge. The final oxygen concentration is almost zero. Analogous to the hydrogen behavior, the oxygen concentration does not change appreciably with position.

Figure 10 shows the concentration of electrolyte (OH^-) in the liquid phase as a function of position and time. Initially the concentration profile is flat at the value set as initial condition. During discharge, the reactions occurring at the nickel (positive) electrode produce OH^- ions and those at the hydrogen (negative) electrode consume OH^- ions. Thus, we see that the electrolyte concentration rises above the initial value in most of the region of the nickel electrode and it decreases toward the hydrogen electrode. However, the gradients in concentration are not large with a variation between 6.0 to 5.65×10^{-3} mol/cm³. Also, electrolyte distribution does not change much over time.

Finally, Fig. 11 shows the profile of the proton concentration in the active material of the nickel electrode. At the beginning of discharge the nickel electrode is fully charged; thus, the proton concentration is at a minimum value. The top plot in Fig. 11 shows the proton concentration right at the onset of discharge and already the con-

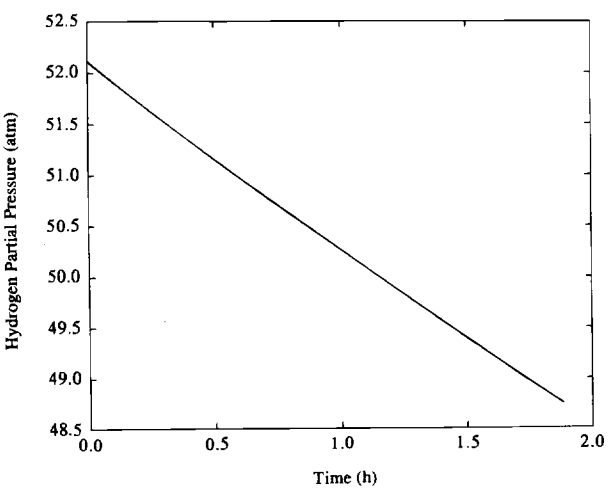

Fig. 8. Simulated hydrogen partial pressure in the head space between the cell stack and the pressure vessel for a discharge rate of −16.25 mA/cm² (C/2).

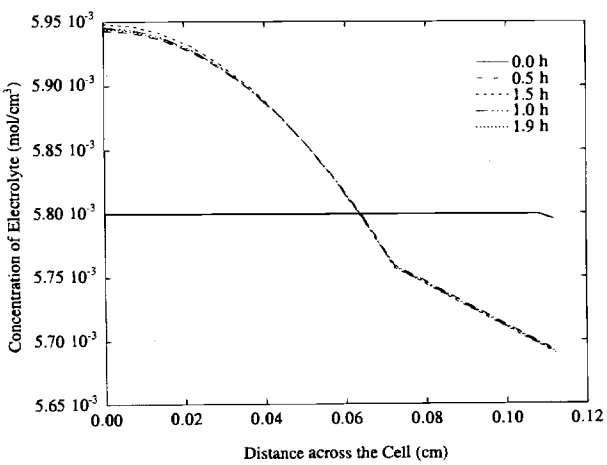

Fig. 10. Simulated concentration of electrolyte distribution for a discharge rate of −16.25 mA/cm² (C/2).

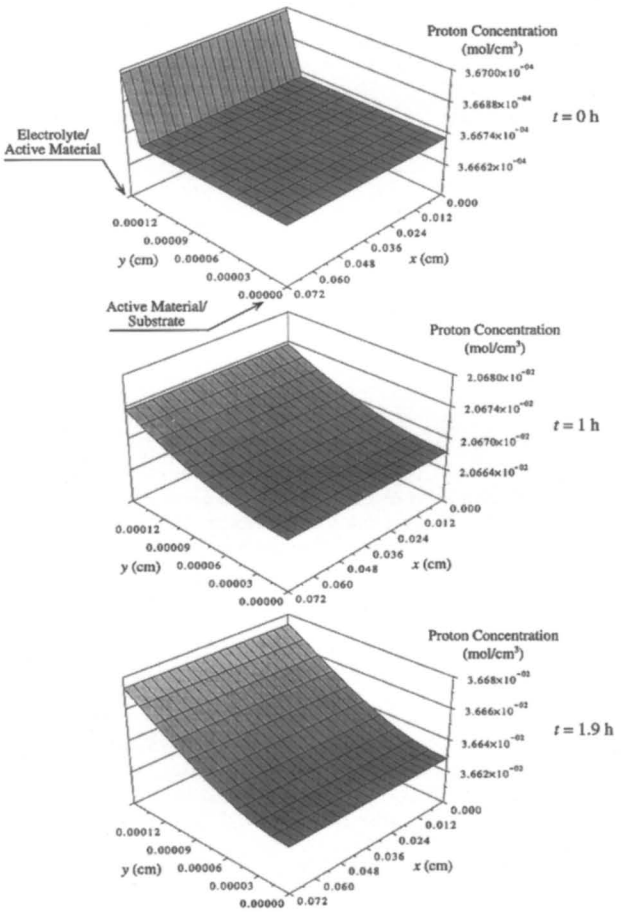

Fig. 11. Simulated proton concentration profiles for a discharge rate of −16.25 mA/cm² (C/2).

centration is increasing at the active material/electrolyte interface (y = 0.00014) due to the main nickel reaction (reaction 1). The center and bottom plots in Fig. 11 show the proton concentration half way into discharge (1 h) and at the end of discharge (1.9 h). In these plots we can see that the overall amount of protons increases with time and that there is a gradient in proton concentration inside the active material caused by the rate of reaction 1 at the surface and the proton diffusion in the bulk of the active material. The proton concentration does not show considerable change in the direction across the electrode (x direction). The potential in the active material is almost constant with respect to time and position, except by the end of the discharge, in which a gradient in the potential in the solid phase in the y direction is developed. This behavior is caused by the decreasing conductivity of the active material as the discharge progresses.

Effect of discharge rate.—The discharge rate or the magnitude of the applied current density affects the behavior of the cell during discharge. Figure 5 shows the simulated cell voltage during discharge operations at various applied currents. As the discharge rate increases (larger currents) the cell voltage decreases because the ohmic drop of the system increases and the discharge time is smaller because the total charge in the nickel electrode is drained sooner.

Figure 12 shows the same voltage curves as Fig. 5 but against the state of discharge. The sharp drop in the cell voltage by the end of discharge takes place at increasingly lower states of discharge as the rate of discharge increases. This behavior is caused by the relative rate between the nickel reaction (reaction 1) and the proton diffusion process in nickel electrode. As the rate of discharge increases (larger applied currents), the rate of reaction of reaction 1 becomes faster with respect to the proton diffusion in the active material. This causes an accumulation of protons on the surface of the active material (active material/electrolyte interface) forcing the potential to drop to maintain the current density used in reaction 1.

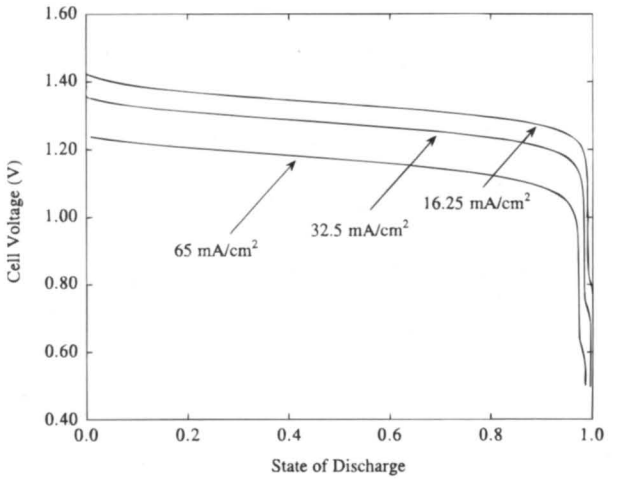

Fig. 12. Simulated cell voltage *vs.* state of discharge for various discharge rates.

The process of proton diffusion in the active material of the nickel electrode affects the utilization of the active material during discharge; that is the discharge efficiency. The voltage curves shown in Fig. 12 show the characteristic decrease in the state-of-discharge at the end of the discharge operation (cutoff voltage of 1.0 V) as the discharge rate is increased. This behavior is caused by a slow proton diffusion process relative to the electrochemical reaction (reaction 1) that takes place on the surface of the active material in the nickel electrode. During discharge, the proton concentration at the surface of the active material ($y = l_y$) increases because of the main electrochemical reaction (reaction 1). As the proton concentration increases the overpotential of the nickel electrode increases causing the cell potential to decrease, and when it reaches the maximum proton concentration, $c_{H^+,max}$, the cell potential drops sharply. The accumulation of protons at the surface of the active material depends on the relative rate between the electrochemical reaction and the proton diffusion into the bulk of the active material. As the discharge rate is increased the electrochemical reaction rate (j_1) increases, the proton concentration at the surface of the active material reaches $c_{H^+,max}$ sooner and a sharp drop in the potential of the cell occurs earlier. Thus, increasingly more active material is left unreacted in the nickel electrode as the discharge rate is increased. Figure 13 shows the proton concentration distribution inside the active material of the nickel electrode at the time when the cell reached a voltage of 1.0 V for two discharge rates, 65 and 16.25 mA/cm². The surface for the higher discharge rate falls below that for the lower discharge rate. This indicates that at the time there is less reacted material in the electrode for the case of higher discharge rate; that is the discharge efficiency is lower for this case. Note also that the lower surface in Fig. 13 exhibits a larger gradient in the y direction because the diffusion resistance is larger relative to the reaction rate at the surface ($y = l_y$).

Second discharge plateau.—The simulated cell voltage during discharge exhibits a second discharge plateau, as shown in Fig. 5. This plateau is caused by the oxygen reduction reaction in the nickel electrode, as shown in Fig. 7. This reaction is favored at a low cell voltage which corresponds to a high negative overpotential in the nickel electrode. Besides the overpotential of the electrode, this reaction requires a certain level of dissolved oxygen to occur as reflected by the kinetic expression for reaction 2 (see Eq. 37). Figure 14 shows the behavior of the simulated cell voltage at various initial oxygen pressure. For the

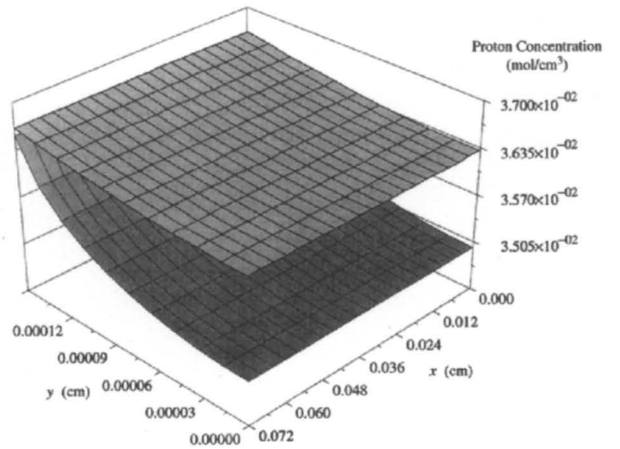

Fig. 13. Simulated proton concentration distribution at a cutoff voltage of 0.9 V for two rates of discharge: −65 mA/cm² and −16.25 mA/cm². The dark and light gray surfaces correspond to −65 and −16.25 mA/cm², respectively.

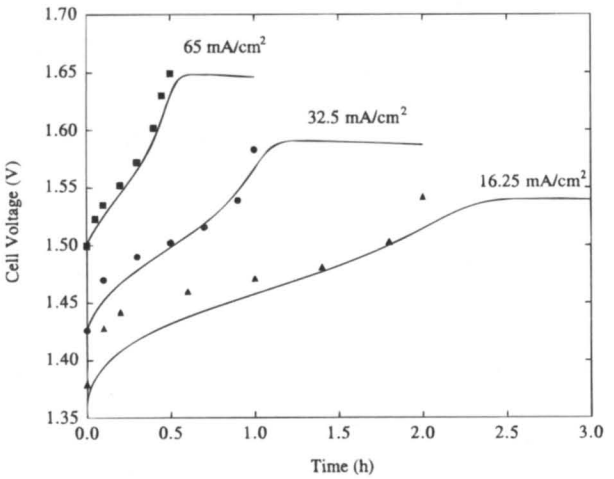

Fig. 15. Comparison of simulated and experimental cell voltage during charge at various rates of discharge. The continuous lines are the simulated curves and the symbols are the experimental data.

values shown in Fig. 14, the oxygen pressure does not affect the curve during the main course of the discharge because oxygen evolution is very small. However, the last portion of the discharge voltage is affected by the oxygen pressure. Specifically, the second discharge plateau occurs earlier and is wider as the oxygen pressure increases. While the voltage stays in the second plateau, oxygen is being consumed (reduced) by reaction 2 and at a smaller rate nickel is being reduced by reaction 1, as shown in Fig. 7. The applied current is shared by this two reactions more evenly as the oxygen pressure decreases; thus, the plateau is more sluggish and lasts for a shorter time for lower oxygen pressures.

The nickel/cadmium battery also exhibits a second discharge plateau.[29] However, models developed for a nickel/cadmium cell[6,7,13] do not show the second plateau, because the mass-transfer resistance to oxygen in those models is very low and they do not include a gas phase. Therefore, oxygen is transported to the negative electrode easily where it is consumed and there is not enough dissolved oxygen accumulated at the nickel electrode for the oxygen reduction to occur by the end of discharge.

Simulations of the charge operation.—The simulated cell voltage agrees with the experimental data, as shown in Fig. 15. The curves for the simulated voltage are somewhat flatter than the experimental curves. The cell voltage rises quickly from its initial value and increases slowly during the main course of charge forming the charge plateau. Then it rises quickly again until it reaches the value for the overcharge plateau.

Figure 16 shows the simulated total cell pressure and experimental data for three charge rates. As with the discharge, the simulated cell pressure shows an excellent agreement with the experimental data; although the experimental data seems to have a less linear behavior as that shown by the simulated curves. The deviations are larger at the lower rates of charge.

Figure 17 shows the predicted current densities used on each reaction during charge. The main reactions on both electrodes (reactions 1 and 4) are the ones dominating the use of the current during the main course of charge. There is a small generation of oxygen (reaction 2) and consumption of hydrogen (reaction 3) in the nickel electrode. As the charge enters the overcharge period (time larger than 2 h), the current density in the nickel electrode switches form being used by reaction 1 to reaction 2 and a small portion is used by reaction 3. In the negative electrode, the side oxygen side reaction 5 is negligible over all the charge process.

Figure 18 shows the simulated hydrogen pressure during charge at a constant current of 16.25 mA/cm². The hydrogen pressure reflects the production of hydrogen by the main reaction in the negative electrode (reaction 4) at a constant rate, as shown in Fig. 17. The hydrogen concen-

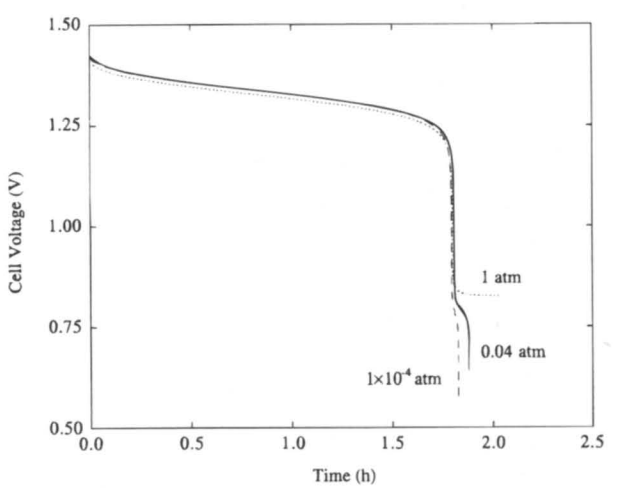

Fig. 14. Simulated cell voltage during discharge at 16.25 mA/cm² for various initial oxygen pressures.

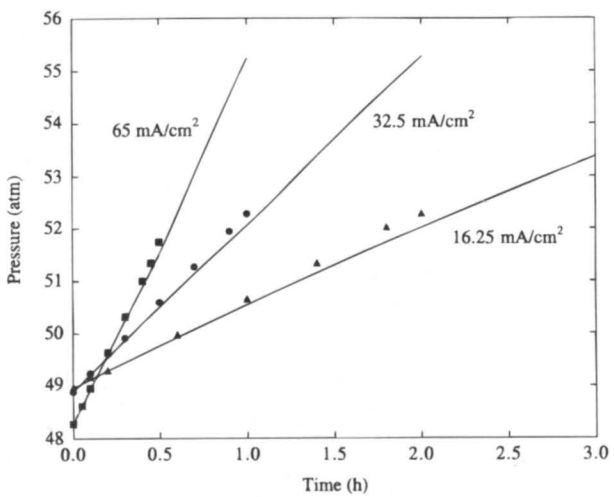

Fig. 16. Comparison of simulated and experimental cell pressure during charge at various rates of discharge.

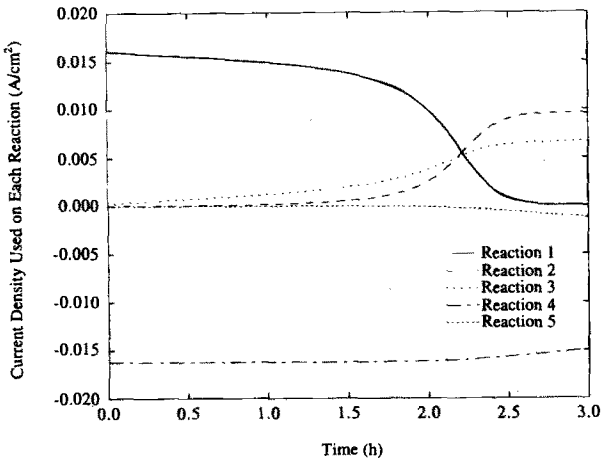

Fig. 17. Simulated current densities used on each reaction in the cell for a charge rate of 16.25 mA/cm² (C/2).

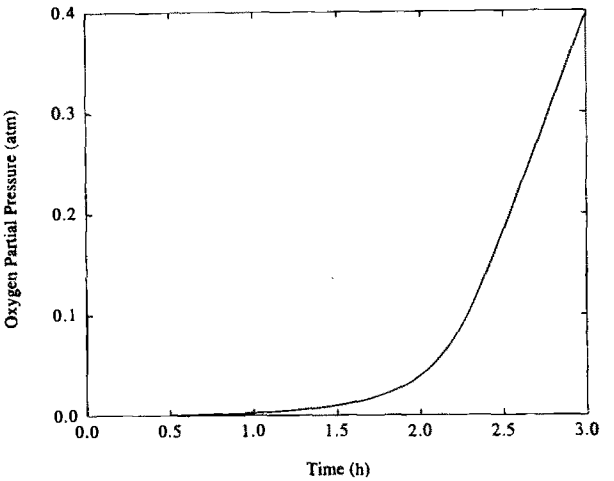

Fig. 19. Simulated oxygen partial pressure in the head space between the cell stack and the pressure vessel for a charge rate of 16.25 mA/cm² (C/2).

tration in the gas phase inside the pores of the cell follows the behavior of the hydrogen pressure, increasing steadily during charge. Similar to the discharge operation, the concentration of hydrogen does not change much with position in the internal gas phase. The hydrogen concentration in the liquid phase also shows a steady increase with time. Near the hydrogen electrode, the hydrogen concentration in the liquid rises because reaction 4 is generating hydrogen.

Figure 19 shows the oxygen pressure in the cell during charge. The oxygen pressure increases slowly during the main course of charge and increases rapidly as the overcharge period starts. The oxygen content in the gas and liquid phases inside the pores of the cell components, follow the same behavior as the oxygen pressure in the cell.

Figure 20 shows the concentration of electrolyte as a function of position and time. During charge, hydroxyl ions are consumed by the reactions in the nickel electrode (reactions 1, 2, and 3) and generated by the main reaction in the hydrogen electrode (reaction 4). Thus, the concentration of electrolyte drops from the initial value in the region of the nickel electrode and rises above the initial value toward the hydrogen electrode. As was the case for the discharge operation, the electrolyte concentration does not change much with time and it falls in a narrow range of values, from 5.65 to 5.9 $\times 10^{-3}$ mol/cm³.

The potential in the liquid phase starts at a positive value and decreases to negative values when overcharge begins (time larger than 2 h). Similar to the discharge operation, the potential does not change much with position. The current density in the liquid phase starts at zero at the current collector of the nickel electrode and increases almost linearly up to the value of the applied current density upon reaching the separator. The change in current density in the nickel electrode is caused by the reactions taking place at that electrode. The proton concentration in the active material of the nickel electrode is high at the beginning of charge and decreases with time because of the main nickel reaction (reaction 1) at the active material/electrolyte interface ($y = l_y$). During charge, the gradient of proton concentration in the y direction is opposite to that obtained during discharge because reaction 1 is advancing in the opposite direction (oxidation of Ni^{2+} to Ni^{3+}). The behavior of the potential in the active material of the nickel electrode is analogous to the discharge case: the potential is almost constant in time and position and it exhibits a gradient in the y direction at the beginning of charge because the active material is on its less conductive state at that moment (fully discharged).

Effect of charge rate.—The rate of charge affects the behavior of the cell voltage over time, as shown in Fig. 15. As the rate of charge increases, the cell is charged faster and the voltage increases because the ohmic losses are larger. Figure 21 shows the simulated final state of charge of the cell against the applied current density. The final

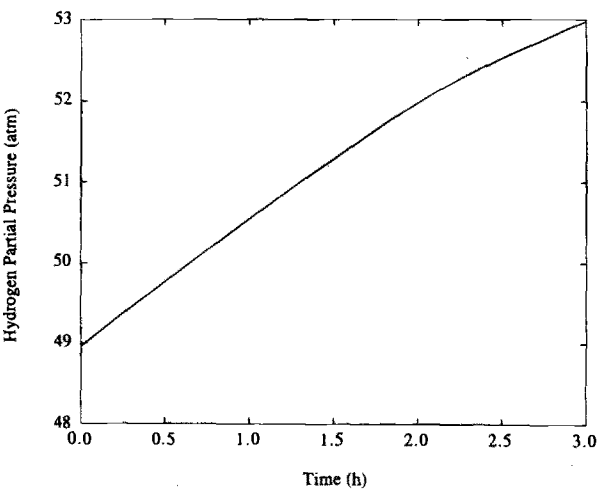

Fig. 18. Simulated hydrogen partial pressure in the head space between the cell stack and the pressure vessel for a charge rate of 16.25 mA/cm² (C/2).

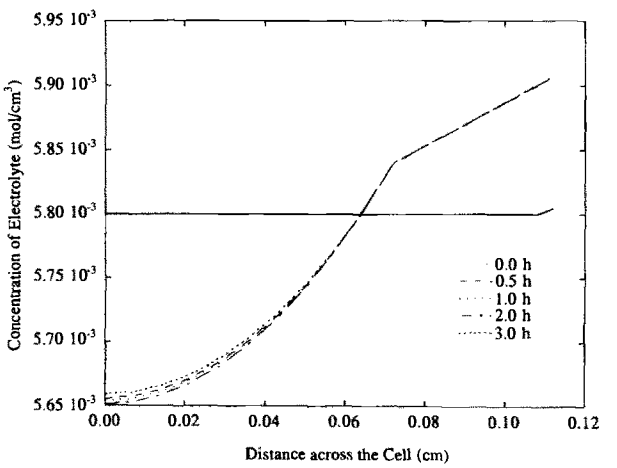

Fig. 20. Simulated concentration of electrolyte distribution for a charge rate of 16.25 mA/cm² (C/2).

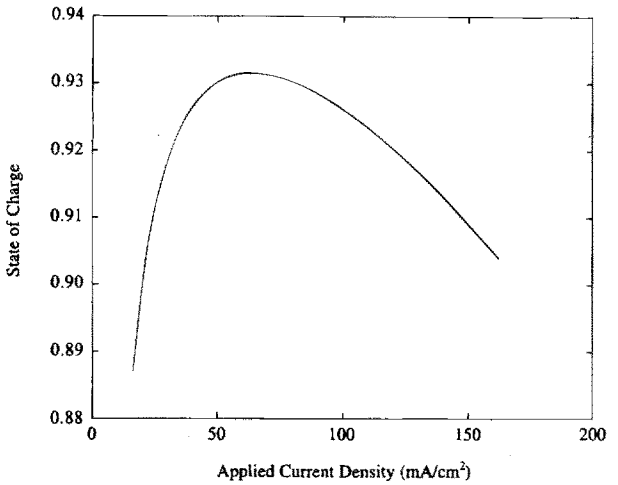

Fig. 21. Simulated final state of charge *vs.* rates of charge.

state of charge was taken at the charging time that corresponds to full theoretical charge based on the charging rate used. For example, for an applied current density of 32.5 mA/cm^2 the final state of charge was computed at 1 h of charging. The final state of charge is a reflection of the charge efficiency of the cell for a given charging rate. Figure 21 shows that there is a maximum in charge efficiency at about 60 mA/cm^2, which corresponds to a charge rate of 1.9 C. For applied currents below 60 mA/cm^2, the final state of charge increases with the applied current density, because reaction 1 is favored over the side reactions 2 and 3 at larger current densities. However, an increase in the charging rate beyond 60 mA/cm^2 leads to a decrease in the charge efficiency because the ohmic losses become very large.

Conclusions

We have developed a mathematical model for a nickel/hydrogen cell to simulate its dynamic behavior. The model was used to study the effect of operating conditions on the cell performance and to study some of the physical phenomena occurring within the cell. The model can be used to evaluate the cell performance under various operating conditions for any given set of design parameters, and thus, determine optimal and safe design and operating conditions for various cell specifications and charge/discharge rates. Various case studies could be performed simply by changing the model input parameters. This could save time and effort if used in place of building and testing different cell designs.

The simulated cell voltage and pressure showed to be in excellent agreement with experimental data, particularly for discharge operation. Simulations for charge operations at various rates, showed that the charging efficiency of the cell has a maximum value with respect to the charging rate. The existence of an optimum charging rate is important for practical applications and the model can be used to find this optimum for particular battery designs.

The model was used to unveil a possible explanation for the existence of the second discharge plateau displayed in real nickel/hydrogen cells. The simulations show that given the proper conditions, oxygen reduction can occur in the nickel electrode and it causes a second discharge plateau at a cell voltage around 0.6 to 0.8 V, depending on the discharge rate. This plateau is affected by the amount of oxygen present in the cell and it tends to disappear for lesser amounts of oxygen. The appearance of second the plateau coincides with what is observed experimentally. The theoretical prediction of the second plateau has not been reported, to our knowledge, by other researchers. The proton diffusion in the active material of the nickel electrode affects the utilization of the active material. If the diffusion coefficient of protons was smaller, such as that reported by,[9] the proton diffusion process could have a larger effect on the utilization of active material as was found for a model of a nickel/cadmium cell.[13]

The model was developed based on several assumptions. First, we assumed that convective effects in the gas phase could be neglected. The simulations obtained using the model showed that the concentration in the gas phase inside the cell pores does not change appreciably across the cell. Therefore, the predicted pressure gradient inside the gas pores was very small leading to expect negligible convection. Adding convective effects to the gas or liquid phase would enhance mass transfer and its effect on the cell behavior would be diminished further. We also assumed that the gas and liquid porosities inside the cell components are constant. This assumption is reasonable for a single operation. However, if the model is used to represent the behavior of the cell over cycling, this assumption may need to be revised. This is because there is electrolyte loss that takes place in real cells on extended cycling resulting in changes in gas and liquid porosities.

The model can be enhanced by incorporating heat-transfer effects, that is, energy balances. In real cells the temperature rises during charge and decreases during discharge. These changes in temperature may affect the kinetics of the reactions and the mass-transfer parameters of the various species in the liquid, solid, and gas phases.

Acknowledgment

The authors acknowledge the financial support of the Office of Research and Development of the United States Central Intelligence Agency. Also, we are grateful to Mr. Yalin Xue for his assistance in the experimental work.

Manuscript received June 27, 1996.

University of South Carolina assisted in meeting the publication costs of this article.

LIST OF SYMBOLS

a_o	specific surface area of the nickel substrate per unit volume in the nickel electrode, cm^2/cm^3
a_{pos}	specific surface area of the solid phase per unit volume in the nickel electrode ($a_{pos} = a_{pos}^{(sl)} + a_{pos}^{(gs)}$), cm^2/cm^3
$a_{pos}^{(sl)}$	specific surface area of the liquid/solid interface per unit volume in the nickel electrode, cm^2/cm^3
$a_{neg}^{(sl)}$	specific surface area of the liquid/solid interface (active area) per unit of cross-sectional area of hydrogen electrode, cm^2/cm^2
$a_{pos}^{(sl)}$	specific surface area of the liquid/gas interface per unit volume in the nickel electrode, cm^2/cm^3
$a_{sep}^{(lg)}$	specific surface area of the liquid/gas interface per unit volume in the separator, cm^2/cm^3
b	parameter for the porosity correction of the diffusion coefficients of the various species in the liquid phase
c_e	concentration of electrolyte, mol/cm^3
c_{H^+}	concentration of protons in the active material of the nickel electrode, mol/cm^3
$c_{H^+,max}$	maximum concentration of protons in the active material of the nickel electrode (fully discharged state), mol/cm^3
$c_{H^+,ref}$	reference concentration of protons in the active material of the nickel electrode, mol/cm^3
$c_{H_2}^{ext}$	concentration of hydrogen gas contained in the head space between the cell stack and the pressure vessel (external gas phase), mol/cm^3
$c_{O_2}^{ext}$	concentration of oxygen gas contained in the head space between the cell stack and the pressure vessel (external gas phase), mol/cm^3
c_o	concentration of solvent, mol/cm^3
c_+	concentration of cations (K^+) in the liquid phase, mol/cm^3
c_-	concentration of anions (OH^-) in the liquid phase, mol/cm^3
$\langle c_e \rangle^{(l)}$	volume averaged concentration of electrolyte, mol/cm^3

$\langle c_{e,ref}\rangle^{(l)}$ reference concentration of electrolyte, mol/cm^3
$\langle c_{H_2}\rangle^{(l)}$ volume averaged concentration of dissolved hydrogen, mol/cm^3
$\langle c_{H_2,ref}\rangle^{(l)}$ reference concentration of dissolved hydrogen, mol/cm^3
$\langle c_{O_2}\rangle^{(l)}$ volume averaged concentration of dissolved oxygen, mol/cm^3
$\langle c_{O_2,ref}\rangle^{(l)}$ reference concentration of dissolved oxygen, mol/cm^3
$\langle c_{H_2}\rangle^{(g)}$ volume averaged concentration of hydrogen gas inside the cell stack, mol/cm^3
$\langle c_{O_2}\rangle^{(g)}$ volume averaged concentration of oxygen gas inside the cell stack, mol/cm^3
d parameter in the porosity correction of the conductivity of electrolyte
D free-stream diffusion coefficient of a concentrated binary electrolyte (KOH) based on a concentration gradient, cm^2/s
D_{integ} free-stream integral diffusion coefficient of a concentrated binary electrolyte (KOH), cm^2/s
$\langle D\rangle^{(l)}$ averaged diffusion coefficient of a binary electrolyte, cm^2/s
$D_i^{(g)}$ diffusion coefficient of species i in the gas phase, cm^2/s
$D_i^{(l)}$ diffusion coefficient of species i in the liquid phase, cm^2/s
$D_i^{(s)}$ diffusion coefficient of species i in the solid phase, cm^2/s
$D_{H^+}^{(s)}$ diffusion coefficient of protons in the active material of the nickel electrode, cm^2/s
F Faraday's constant, 96,487 C/eq
$f_\pm$ mean molar activity coefficient of the electrolyte
$i^{(l)}$ x-component of the current density in the liquid, A/cm^2
i_{cell} current density applied to the cell, A/cm^2
j_k local current density due to reaction k taking place in the liquid/solid interface, A/cm^2
$j_{ok,\,ref}$ exchange current density for reaction k at reference conditions, A/cm^2
$\langle j_k\rangle^{(ls)}$ averaged local current density due to reaction k taking place in the liquid/solid interface, A/cm^2
$K_{e,i}$ equilibrium constant relating the concentration of species i in the liquid and the gas phase (constant from Henry's law)
k_i^{ext} rate constant for the molar flux of species j between the internal and external gas phases ($(-N_{j,r}^{(g)})|_{r_c}$) in region i, mol/atm cm^2 s
k_{tef}^{ext} rate constant for the molar flux of species j between the internal and external gas phases at the back of the hydrogen electrode, mol/atm cm^2 s
$k_i^{(lg)}$ rate constant for the molar flux of species i between the liquid phase and gas phase in the pores of the cell components ($r_i^{(lg)}$), cm/s
$k_i^{(lg,ext)}$ rate constant for the molar flux of species i between the liquid phase at the back of the hydrogen electrode and gas phase right outside the back of the hydrogen electrode, cm/s
l_1 x-coordinate for the location of the interface between the nickel electrode and the separator (thickness of the nickel electrode), cm
l_2 x-coordinate for the location of the interface between the separator and the hydrogen electrode ($l_2 - l_1$ is the thickness of the separator), cm
l_y thickness of the active material layer in the nickel electrode, cm
m molality of the electrolyte, mol/kg
$n_{H_2}^{ext}$ number of moles of hydrogen gas contained in the head space between the cell stack and the pressure vessel (external gas phase), mol
$n_{O_2}^{ext}$ number of moles of oxygen gas contained in the head space between the cell stack and the pressure vessel (external gas phase), mol
$p_{H_2,ref}$ reference partial pressure of hydrogen, atm
$p_{O_2,ref}$ reference partial pressure of oxygen, atm
Q charge in the nickel electrode, C/cm^2
Q_{max} maximum theoretical charge of the nickel electrode, C/cm^2
R universal gas constant, 8.3143 J/mol K
r_c radius of the cell stack, cm
SOC state of charge of the cell
SOD state of discharge of the cell
t time, s
T temperature, K
t_i^* transference number of species i with respect to $\mathbf{v}^*$
V^{ext} volume of the head space between the cell stack and the pressure vessel (external gas space), cm^3
$\mathbf{v}^*$ molar-average velocity of the solution, cm/s
x spatial coordinate across the cell, cm
y radial spatial coordinate in the active material in the nickel electrode, cm
y_o radius of the cylinder representing the nickel substrate in the nickel electrode, cm
z_i ionic charge number or valence of species i, eq/mol

Greek

α_{ak} anodic transfer coefficient for reaction k
α_{ck} cathodic transfer coefficient for reaction k
$\epsilon_{o,pos}$ porosity of the nickel substrate before impregnation of active material
$\epsilon_{pos}^{(g)}$ gas porosity in the positive nickel electrode
$\epsilon_{sep}^{(g)}$ gas porosity in the separator
$\epsilon_{pos}^{(l)}$ liquid porosity in the positive nickel electrode
$\epsilon_{sep}^{(l)}$ liquid porosity in the separator
$\phi^{(s)}$ electric potential in the solid phase, V
$\langle\phi\rangle^{(l)}$ averaged electric potential in the liquid phase, V
ϕ_{H_2} potential in the hydrogen electrode, V
$\phi_{eq\ k,\ ref}$ equilibrium potential of reaction k evaluated at reference conditions, V
ϕ_{sub} potential in the nickel substrate of the nickel electrode, V
$\gamma_\pm$ mean molal activity coefficient of the electrolyte
η_k overpotential for reaction k, V
κ free-stream conductivity of the electrolyte, S/cm
$\langle\kappa\rangle^{(l)}$ volume averaged conductivity of the electrolyte, S/cm
ν_+ number of moles of cations into which a molecule of electrolyte dissociates
ν_- number of moles of anions into which a molecule of electrolyte dissociates
ρ mass density of the solution, g/cm^3
ρ_i mass density of species i, g/cm^3
$\sigma^{(s)}$ electrical conductivity of the solid phase in the porous electrode, S/cm

REFERENCES

1. J. D. Dunlop, G. M. Rao, and T. Y. Yi, *NASA Handbook for Nickel-Hydrogen Batteries,* NASA reference publication 1314 (1993).
2. K. Micka and I. Rousar, *Electrochim. Acta*, **25,** 1085 (1980).
3. K. Micka and I. Rousar, *ibid.*, **27,** 765 (1982).
4. J. Bouet, F. Richard, and P. Blanchard, in *Nickel Hydroxide Electrodes*, D. A. Corrigan and A. H. Zimmerman, Editors, PV 90-4, p. 260, The Electrochemical Society Proceedings Series, Pennington, NJ (1989).
5. K. W. Choi and N. P. Yao, in *Battery Design and Optimization*, S. Gross, Editor, PV 79-1, p. 62, The Electrochemical Society Proceedings Series, Pennington, NJ (1979).
6. D. Fan and R. E. White, *This Journal*, **138,** 17 (1991).
7. D. Fan and R. E. White, *ibid.*, **138,** 2952 (1991).
8. Z. Mao, P. De Vidts, R. E. White, and J. Newman, *ibid.*, **141,** 54 (1994).
9. D. M. MacArthur, *ibid.*, **117,** 729 (1970).
10. G. W. Briggs and P. R. Snodin, *Electrochim. Acta*, **27,** 565 (1982).
11. A. H. Zimmerman and P. K. Effa, *This Journal*, **131,** 709 (1984).
12. C. Zhang and S.-M. Park, *ibid.*, **134,** 2966 (1987).
13. P. De Vidts and R. E. White, *ibid.*, **142,** 1509 (1995).
14. A. H. Zimmerman, in *Nickel Hydroxide Electrodes*, D. A. Corrigan, A. H. Zimmerman, Editors, PV 90-4, p. 311, The Electrochemical Society Proceedings Series, Pennington, NJ (1989).
15. J. S. Newman, *Electrochemical Systems,* 2nd ed., Prentice-Hall, Englewood Cliffs, NJ (1991).
16. J. C. Slattery, *Momentum, Energy, and Mass Transfer in Continua*, 2nd ed., Robert E. Krieger Publ. Co., Huntington, NY (1981).
17. P. De Vidts, Ph.D. Thesis, Texas A&M University, College Station, TX (1995).

18. V. M. M. Lobo, *Handbook of Electrolyte Solutions*, Vol. A, Elsevier, New York (1989).
19. S. Motupally, C. C. Streinz, and J. W. Weidner, *This Journal*, **142**, 1401 (1995).
20. K. E. Brenan, S. L. Campbell, and L. R. Petzold, *Numerical Solution of Initial-Value Problems in Differential-Algebraic Equations*, North-Holland, New York (1989).
21. W. E. Schiesser, *The Numerical Method of Lines: Integration of Partial Differential Equations*, Academic Press, Inc., San Diego, CA (1991).
22. R. E. Meredith and C. W. Tobias, in *Advances in Electrochemistry and Electrochemical Engineering*, *2*, C. W. Tobias, Editor, p. 15, Interscience Publ., New York (1962).
23. M. Kimble, Ph.D. Thesis, Texas A&M University, College Station, TX (1991).
24. E. L. Cussler, *Diffusion: Mass Transfer in Fluid Systems*, Cambridge University Press, New York (1984).
25. M. K. Tham, R. D. J. Walker, and K. E. Gubbins, *J. Phys. Chem.*, **74**, 1747 (1970).
26. K. E. Gubbins and R. D. J. Walker, *This Journal*, **112**, 469 (1965).
27. P. C. Milner and U. B. Thomas, in *Advances in Electrochemistry and Electrochemical Engineering*, *5*, C. W. Tobias, Editor, p. 1, John Wiley & Sons, Inc., New York (1967).
28. B. V. Tilak, P. W. T. Lu, J. E. Colman, and S. Srinivasan, in *Comprehensive Treatise of Electrochemistry*, *2*, J. O'M. Bockris, B. E. Conway, E. Yeager, R. E. White, Editors, p. 1, Plenum Press, New York (1984).
29. W. R. Scott and D. W. Rusta, *Sealed-Cell Nickel-Cadmium Battery Applications Manual*, NASA Reference Publication 1052 (1979).
30. J.-G. Le Helloco, H. Bojkov, A. Parthasarathy, S. Srinivasan, and A. J. Appleby, in *Hydrogen Storage Materials, Batteries, and Electrochemistry*, D. A. Corrigan and S. Srinivasan, Editors, PV 92-5, p. 417, The Electrochemical Society Proceedings Series, Inc., Pennington, NJ (1992).